High-resolution upper Maastrichtian carbon isotope stratigraphy of terrestrial organic matter from northern Japan

Ko Nifuku[a,b,*], Hajime Naruse[a, c], Minoru Ikehara[d]

[a]*Division of Earth and Planetary Sciences, Graduate School of Science, Kyoto University, Kitashirakawa Oiwake-cho, Sakyo-ku, Kyoto 606-8502, Japan*

[b]*Present address: INPEX Corporation, Akasaka Biz Tower 5-3-1 Akasaka, Minato-ku, Tokyo 107-6332, Japan*

[c]*E-mail: naruse@kueps.kyoto-u.ac.jp*

[d]*Center for Advanced Marine Core Research, Kochi University, 200 Monobe-otsu, Nankoku, Kochi 783-8502, Japan. E-mail: ikehara@kochi-u.ac.jp*

[*]Corresponding author: Ko Nifuku, INPEX Corporation, Akasaka Biz Tower 5-3-1 Akasaka, Minato-ku, Tokyo 107-6332, Japan. E-mail: nifukuko@gmail.com, Tel: +81-3-5572-0362, Fax: +81-3-5572-0239.

ABSTRACT

High-resolution stable carbon isotope stratigraphy of terrestrial organic matter was established for the upper Maastrichtian Senpohshi Formation of the Nemuro Group in eastern Hokkaido, northern Japan. The Senpohshi Formation, approximately 1,300 m thick, is dominated by hemipelagic mudstone deposited along an active margin in the North Pacific region. Microscopic observations of extracted kerogen samples from the formation revealed the presence of sedimentary organic matter (SOM), predominantly phytoclasts and a minor amount of non-fluorescent amorphous organic matter, indicating material of a terrestrial higher plant origin. The atomic hydrogen/carbon ratios of the kerogen samples indicated a coalification rank at the anthracite stage or below. Therefore, the stable carbon isotope values of the bulk SOM obtained for the Senpohshi Formation represent the unmodified, original values of terrestrial organic matter. The stable carbon isotope profile reconstructed for the Formation provides the first high-resolution terrestrial record of the Mid-Maastrichtian Event (MME), which is comparable to high-resolution marine carbon isotope data from other sections. The carbon isotopic signatures defined by the marine records are recognized in the terrestrial data from the Formation, especially in middle to upper part of the event. However, the terrestrial record showed a discrepancy from the marine data in the lower part of the MME, suggesting local variation

of the hinterland environment in the North Pacific region. This study provides new insight into environmental changes during the late Maastrichtian by establishing a detailed carbon isotope record of terrestrial materials.

Keywords: Carbon isotope stratigraphy; terrestrial organic matter; Mid-Maastrichtian Event; hinterland environment; Nemuro Group; North Pacific region

1. Introduction

The Maastrichtian Age is a time marked by extensive environmental changes. Third-order cycle, high-amplitude falls in sea level are recognized in the Maastrichtian, which can be superimposed over the long-term sea-level drop from the latest Cretaceous through the Paleogene (Haq et al., 1987; Crampton et al., 2006; Simmons et al., 2007; Kominz et al., 2008). The Maastrichtian is also characterized by short-term climatic cooling and warming events accompanied by the long-term climatic cooling in the latest Cretaceous (Barrera and Huber, 1990; Barrera and Savin, 1999; Frank and Arthur, 1999; Li and Keller, 1999; Huber et al., 2002; Frank et al., 2005; MacLeod et al., 2005; Isaza-Londoño et al., 2006; Friedrich et al., 2009; Thibault and Gardin, 2010). Furthermore, changes in thermohaline circulation during the Maastrichtian have been suggested, although the mechanism and characteristics remain controversial (MacLeod and Huber, 1996; Barrera et al., 1997; Barrera and Savin, 1999; Frank and Arthur, 1999; MacLeod et al., 2000; Frank et al., 2005; Pucéat et al., 2005; Donnadieu et al., 2006; Hunter et al., 2008; MacLeod et al., 2011; Murphy and Thomas, 2012; Robinson and Vance, 2012; Robinson et al., 2012; Jung et al., 2013; Voigt et al., 2013; Moiroud et al., 2016; Farnsworth et al., 2019; Haynes et al., 2020; Ladant et al., 2020).

Environmental changes during the Maastrichtian likely resulted in significant biotic events. For example, evidence from this stage suggests widespread inoceramid bivalve extinction in the mid-Maastrichtian (Ward et al., 1991; MacLeod et al., 1996), rudist reef collapse in tropical regions (Johnson and Kauffman, 1990, 1996; Johnson et al., 1996), and an increase in provinciality in plankton microfossil assemblages (Shafik, 1990; Huber, 1992; Huber and Watkins, 1992; Burnett, 1998; Lees, 2002; Thibault et al., 2012a, b). Moreover, there is evidence of latitudinal migration of calcareous plankton (e.g., the calcareous nannofossils *Nephrolithus frequens* and *Micula murus* and the planktonic foraminifer *Abathomphalus mayaroensis*) during the Maastrichtian (Pospichal and Wise, 1990; Huber, 1992; Huber and Watkins, 1992; Nifuku et al., 2009; Thibault et al., 2010; Voigt et al., 2012). The present consensus is that sea-level fall, climatic cooling, and changes in thermohaline circulation played important roles in these biotic events (MacLeod and Huber, 1996; Barrera et al., 1997; Barrera and Savin, 1999; Frank and Arthur, 1999; MacLeod et al., 2000; Frank et al., 2005; Pucéat et al., 2005; Donnadieu et al., 2006; Hunter et al., 2008; MacLeod et al., 2011; Murphy and Thomas, 2012; Robinson and Vance, 2012; Robinson et al., 2012; Jung et al., 2013; Voigt et al., 2013; Moiroud et al., 2016; Farnsworth et a., 2019; Haynes et al., 2020; Ladant et al., 2020).

Records of stratigraphic trends in stable carbon isotopes are useful tools for investigating paleoenvironments. A variety of marine and terrestrial-origin materials has been measured for this purpose (e.g., bulk carbonate rock, calcareous fossil, bulk sedimentary organic matter (SOM), and fossil wood fragments). Global paleoenvironmental events are recorded in carbon isotope profiles, where measured values are representative of the isotopic composition of ocean-atmosphere reservoirs. Perturbation of global carbon isotope composition may be caused by the environmental events, such as extensive organic carbon burial (Scholle and Arthur, 1980; Jenkyns, 1988), CO_2 emission by massive volcanic events (Hesselbo et al., 2002), or large-scale dissociation of methane hydrate (Dickens et al., 1995). The local environment can also control the stable carbon isotope profile. For instance, carbon isotope values of marine carbonate may be influenced by the local factors such as fluvial runoff, primary productivity, or bottom water circulation (Immenhauser et al., 2008; Wendler, 2013). Hinterland climate can affect the isotopic composition in terrestrial organic matter (Farquhar et al., 1980; Ramesh et al., 1986; Körner et al., 1988; Leavitt, 1993; Feng and Epstein, 1995; Lipp et al., 1996; Pendall et al., 1999; Schleser et al., 1999; Edwards et al., 2000). Therefore, stable carbon isotope composition can record global to local scale changes of the paleoenvironment.

Stable carbon isotope stratigraphy has been widely established in the Maastrichtian sections (e.g. Li ad Keller, 1998a, b; Barrera and Savin, 1999; Hasegawa et al., 2003; Nordt et al., 2003: Friedrich et al., 2009; Voigt et al., 2010; Batenburg et al., 2012; Thibault et al., 2012a, b; Voigt et al., 2012; Jung et al., 2012; Falzoni et al., 2016; Salazar-Jaramillo et al. 2016; Dameron et al., 2017; Batenburg et al., 2018). Several prominent carbon isotope events have been recognized in previous research. The Campanian–Maastrichtian Boundary Event (CMBE) is characterized by a relatively prolonged negative excursion from the latest Campanian to the early Maastrichtian (Barrera and Savin, 1999). The Mid-Maastrichtian Event (MME) is characterized by two positive peaks interrupted by a negative trough with multiple short-term negative excursions (Voigt et al., 2012). Carbon isotope values dropped abruptly at the end of the Cretaceous, which is marked by the Cretaceous–Paleogene Boundary Event (KPgE) (Hsü et al., 1982; Perch-Nielsen et al., 1982; Zachos and Arthur, 1986; Keller and Lindinger, 1989). These events are global phenomena indicated by carbon isotope events simultaneously recorded in diverse materials from various regions (Hasegawa et al., 2003; Wendler, 2013; Salazar-Jaramillo et al., 2016). In addition to these events, recent high-resolution carbon isotope stratigraphy reveals the presence of further carbon isotope events in the Maastrichtian,

which are correlated globally (Jung et al., 2012; Thibault et al., 2012a, b; Voigt et al., 2012; Wendler, 2013; Batenburg et al., 2018).

Most of the carbon isotope profiles from the Maastrichtian sections are derived from marine materials, which are bulk carbonate rocks (Zachos et al., 1985; Corfield et al., 1991; Stoll and Schrag, 2000; Voigt et al., 2010; Wendler et al., 2011; Jung et al., 2012; Thibault et al., 2012a, b; Voigt et al., 2012; Batenburg et al., 2018) and single-species of calcareous microfossils (Zachos et al., 1985, 1989; Barrera and Huber, 1990; D'Hondt and Lindinger, 1994; Corfield and Norris, 1996; Li and Keller, 1998a, b; Barrera and Savin, 1999; MacLeod and Huber, 2001; Friedrich et al., 2009).

In contrast, the carbon isotope profile is rarely obtained from terrestrial materials. Hasegawa et al. (2003) established stable carbon isotope stratigraphy from terrestrial organic matter for the upper Cenomanian through upper Maastrichtian (up to polarity chron C30n) from Naiba section in Sakhalin Island, Russia. Salazar-Jaramillo et al. (2016) presented the profile for terrestrial organic matter in the lower Cantwell Formation, Alaska, which covered the carbon isotope events CMBE and MME. Nordt et al. (2003) obtained stable carbon isotope stratigraphy from pedogenic carbonate in Tornillo Basin, Texas, which ranged from the upper Campanian through the Danian. However, the temporal resolution of the isotope stratigraphies obtained from terrestrial material is much

lower than that of the recently established high-resolution carbon isotope stratigraphy from marine carbonates (Batenburg et al., 2012; Jung et al., 2012; Thibault et al., 2012a, b; Voigt et al., 2012; Batenburg et al., 2018). Moreover, limitation of the age control in the lower Cantwell Formation and Tornillo Basin makes it difficult to correlate the terrestrial carbon isotope profiles to the high-resolution marine records. Therefore, acquisition of a high-resolution carbon isotope data from terrestrial material would provide a comprehensive view on isotopic composition of ocean-atmosphere reservoirs during the Maastrichtian. In addition, a detailed terrestrial carbon isotope record would give an insight into terrestrial environment during the stage, which is rarely investigated compared with the paleoenvironment in marine realm. The terrestrial data should be obtained from the sections where sufficient age control has been established because it enables accurate stratigraphic correlation between the terrestrial and marine records.

Here, we established a Maastrichtian carbon isotope stratigraphy of terrestrial material at a higher resolution than the previous study on terrestrial materials (Hasegawa et al., 2003; Nordt et al., 2003; Salazar-Jaramillo et al., 2016). We researched the upper Maastrichtian Senpohshi Formation in eastern Hokkaido, northern Japan (Figs. 1 and 2). The rapid sedimentation rate of the formation enabled us to establish a high-resolution carbon isotope stratigraphy of terrestrial-origin SOM. Furthermore, the

146 magnetostratigraphy established in the section provides reliable stratigraphic markers for
147 global correlations (Nifuku et al., 2009). In this paper, we discuss the carbon isotope
148 stratigraphy derived from the Senpohshi Formation and its comparison with the carbon
149 isotope profiles from other sections.
150

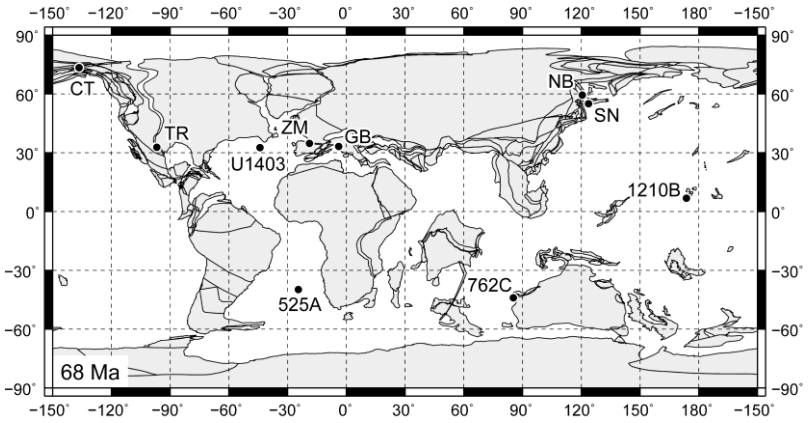

151

152 **Fig. 1.** Paleogeographic map of the late Maastrichtian (68 Ma; modified after Hay et al., 1999,
153 https://www.odsn.de/odsn/services/paleomap/adv_map.html) showing the location of the sections
154 used in this study. SN: Senphoshi Formation of the Nemuro Group, northern Japan; NB: Naiba section,
155 Sakhalin, eastern Russia; GB: Bottaccione Gorge and the Contessa Highway sections at Gubbio, Italy;
156 ZM: Zumaia section, Basque country, Northern Spain; TR: Aguja, Javelina, and Black Peaks
157 Formations in the Tornillo Basin, Texas, US; CT: lower Cantwell Formation, Alaska, US. Numbers
158 indicate DSDP, ODP, and IODP sites (DSDP Site 525A, South Atlantic Ocean; ODP Site 762C, Indian
159 Ocean; ODP Site 1210B, equatorial Pacific Ocean; IODP Site U1403, Newfoundland Margin).
160

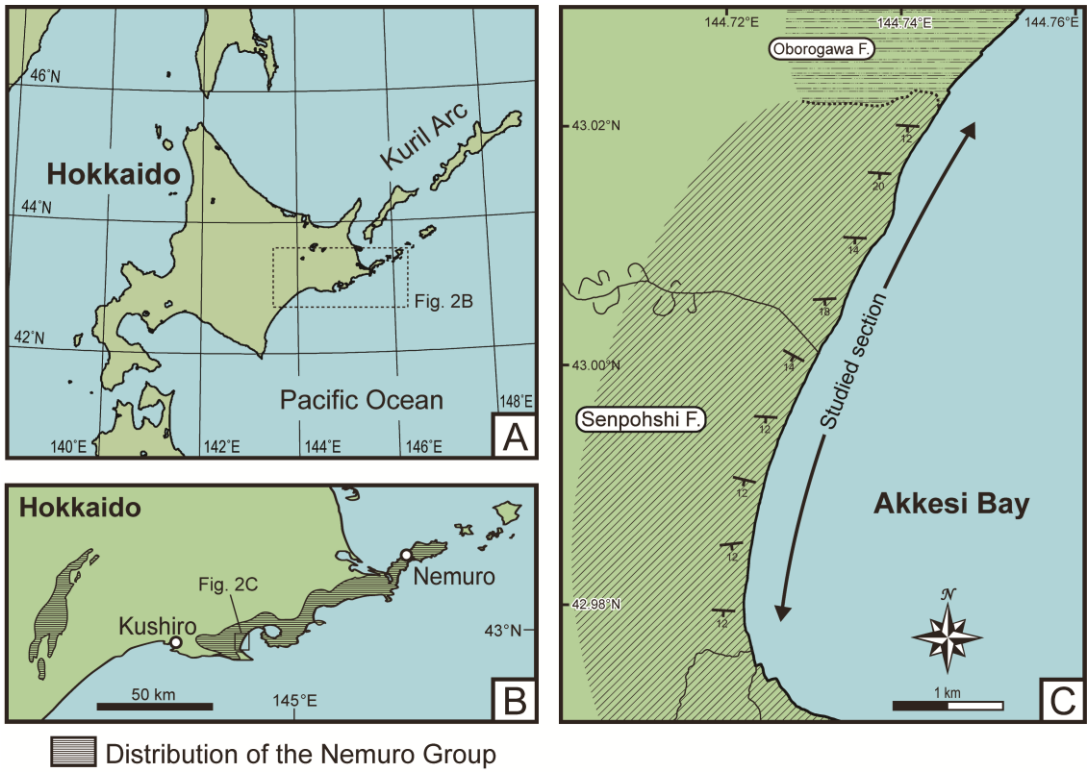

Fig. 2. Index maps showing (A) the location of Hokkaido and (B) the distribution of the Nemuro Group, and (C) location of the studied section.

2. Geological setting and chronology

2.1. Geological setting

The Senpohshi Formation is a part of the Cretaceous–Paleogene Nemuro Group, which is exposed in eastern Hokkaido, northern Japan (Fig. 2). The Nemuro Group is mainly composed of hemipelagic mudstones and sediment gravity flow deposits, such as turbidites and submarine slumps deposits (Kiminami, 1978; Naruse, 2003). The Group is interpreted to represent deposits of the forearc basin located adjacent to the Paleo-Kuril

arc (Kiminami, 1983; Kimura, 1994). Plate tectonic reconstruction suggested the basin located in the North Pacific region, though the paleolatitude during the Late Cretaceous is still controversial (Kimura, 1994; Bazhenov and Burtman, 1994; Fujiwara et al., 1995; Bazhenov et al., 2001; Nifuku et al., 2009; Katagiri et al., 2020).

The Senpohshi Formation is widely exposed along the western coast of Akkeshi Bay, eastern Hokkaido (Fig. 2C). It conformably overlies the Oborogawa Formation and is unconformably overlain by the Shiomi Formation (Asano, 1962; Okada et al., 1987). Bedding within the formation is homoclinal, dipping 10°–20° to the south. The thickness of the formation exceeds 1,270 m (the upper boundary is not exposed). No large-scale faults or tectonic folding are recognized. The formation mainly consists of weakly bioturbated, dark grey mudstone layers occasionally intercalated with sandstone laminae or thin beds of sandstones (~1.0 cm), which are interpreted as sediment gravity flow deposits (Fig. 3). Thin slump deposits occur locally. These sedimentary features suggest that the formation was deposited at the base of a submarine slope (Naruse, 2003).

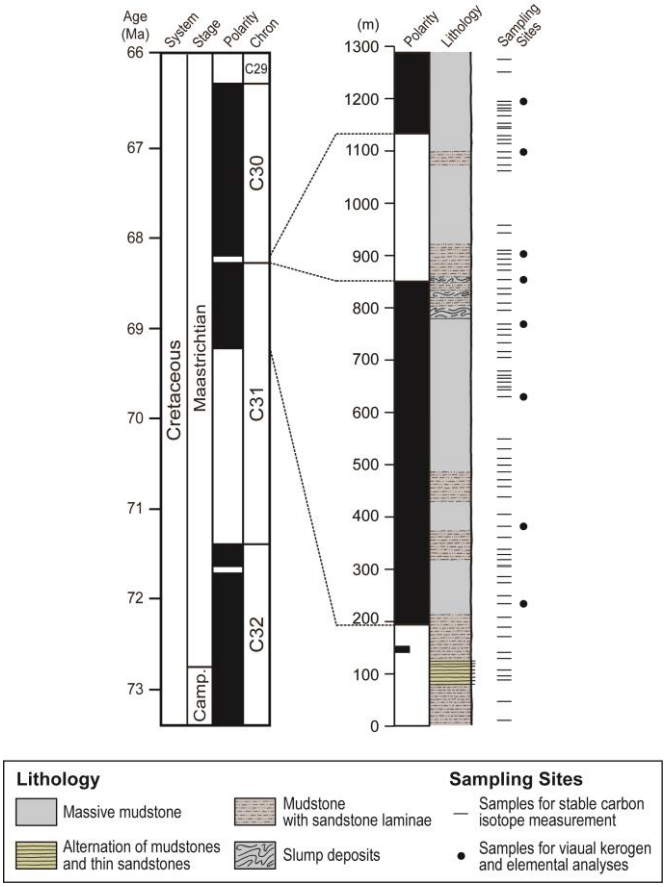

187

188 **Fig. 3.** Lithology and magnetostratigraphy (after Nifuku et al., 2009) of the Senpohshi Formation.

189 Correlation with the astronomically calibrated magnetostratigraphic time scale (Option 2 of Husson et

190 al., 2011) is shown. Stratigraphic position of the sampling sites is also indicated in the figure.

191

192 *2.2. Chronology*

193 The Senpohshi Formation is assigned to the Maastrichtian based on biostratigraphy

194 and magnetostratigraphy. Maastrichtian index fossils have been found in this formation.

195 Naruse et al. (2000) and Nifuku et al. (2009) reported the ammonite *Pachydiscus*

196 *flexuosus* from the lower part of the formation. This species is commonly found in

197 Maastrichtian successions in southern Sakhalin and Hokkaido (Maeda and Shigeta, 2005;
198 Maeda et al., 2005). Shigeta et al. (2015) reported an ammonite fossil assemblage from
199 the same section including *Gaudryceras makarovense*, *Gaudryceras* cf. *seymouriense*,
200 *Anagaudryceras matsumotoi*, and *Diplomoceras* cf. *notabile* fossils, which are indicative
201 of the mid to upper Maastrichtian. Moreover, Nifuku et al. (2009) reported the occurrence
202 of *"Inoceramus" awajiensis*, a known Maastrichtian index fossil of the northwest Pacific
203 (Toshimitsu et al., 1995), in the middle part of the formation. Okada et al. (1987) reported
204 the occurrence of the calcareous nannofossil *Nephrolithus frequens*, a known global index
205 fossil of the upper Maastrichtian (Burnett, 1998), in the upper part of the formation.
206 Moreover, the planktonic foraminifera *Globotruncanella petaloidea*, also an index fossil
207 of the Maastrichtian (Caron, 1985), has been reported from the upper part of the formation
208 (Yamada, 1984).

209 Nifuku et al. (2009) established the magnetostratigraphy of the formation, identifying
210 four magnetozones. Considering the relationship between the biostratigraphy and
211 magnetostratigraphy of the formation, the magnetozones were correlated with polarity
212 chrons C31r–C30n, corresponding to the upper part of the lower Maastrichtian to the
213 upper Maastrichtian (Fig. 3, Table 1).

Table 1. Stratigraphic positions of polarity chron boundaries in the Senpohshi Formation (Nifuku et al., 2009).

Polarity Chron Boundary	Stratigraphic height (m)
C30n/C30r	1118
C30r/C31n	841
C31n/C31r	190

3. Materials and methods

Samples were collected from 72 horizons within the Senpohshi Formation at stratigraphic intervals of 2–104 m (average 18 m), depending on exposure (Fig. 3). All samples were taken from hemipelagic mudstone. Turbidites and slump deposits were excluded from sampling and analysis.

To investigate the content of the sedimentary organic matter (SOM) and to evaluate the degree of thermal maturation, kerogen samples were extracted from eight mudstone samples. First, moderately crushed samples were immersed repeatedly in HCl and HF and then treated with a surfactant. Processed samples were then centrifuged using $ZnCl_2$ solution (specific gravity, 2.00) to extract the kerogen. To obtain estimates of the SOM content, the extracted kerogen samples were observed under transmitted and fluorescent (blue UV) light following a modified version of the classification scheme for organic particles proposed by Tyson (1995); in our study, amorphous organic matter was divided

into nonfluorescent amorphous organic matter (NFA), weakly fluorescent amorphous organic matter (WFA), and fluorescent amorphous organic matter (FA), based on fluorescence properties. The relative abundance of each type was determined by counting 500 points at intervals of 100 μm under transmitted and fluorescent light. To evaluate the degree of thermal diagenesis, we determined the atomic hydrogen/carbon ratio (H/C ratio) of the bulk extracted kerogen samples using a Finnigan FlashEA 1112 elemental analyzer.

Stable carbon isotopic ratios of the bulk SOM and the total organic carbon (TOC) content were analyzed from the mudstone samples. Powdered mudstone samples were treated with HCl to remove carbonate minerals before analysis. The stable carbon isotope ratios and TOC contents of the treated bulk mudstone samples were measured using a mass spectrometer coupled with an elemental analyzer (Finnigan FlashEA 1112, ConFloIII, and DELTA Plus Advantage). Stable carbon isotopic ratios were expressed in δ-notation relative to the PDB standard:

$$\delta^{13}C\ (‰) = (R_{sample}/R_{standard} - 1) \times 1000 \quad (1)$$

where $R = {}^{13}C/{}^{12}C$. L-Histidine (SHOKO Science Co., Ltd.) was used as an internal laboratory standard and the stable carbon isotopic composition was –10.19‰. Repeated analysis of the laboratory standard indicated an overall uncertainty within ±0.25‰ (1σ).

4. Results

4.1. Constituents and H/C ratio of SOM

Microscopic observations revealed that the SOM within the Senpohshi Formation is dominated by phytoclasts with a minor amount of amorphous organic matter (Figs. 4 and 5, Table 2). These two elements made up more than 99% of the SOM in each sample. Phytoclasts constituted 78.4%–98.6% of the SOM and were classified predominantly as translucent phytoclasts without a definitive biostructure (44.4%–62.4%) and opaque phytoclasts (31.2%–54.2%). Translucent phytoclasts with a definitive biostructure are rare, and they are dominantly represented by cuticles. Amorphous organic matter constituted 1.4%–21.4% of the SOM. The NFA was the dominant type of amorphous organic matter, whereas there were very small amounts of WFA and FA. Palynomorphs were rare in the SOM and accounted for less than 0.6% of the SOM.

The average atomic H/C value of the extracted kerogen samples was 0.64 and ranged from 0.47 to 0.81 (Table 3).

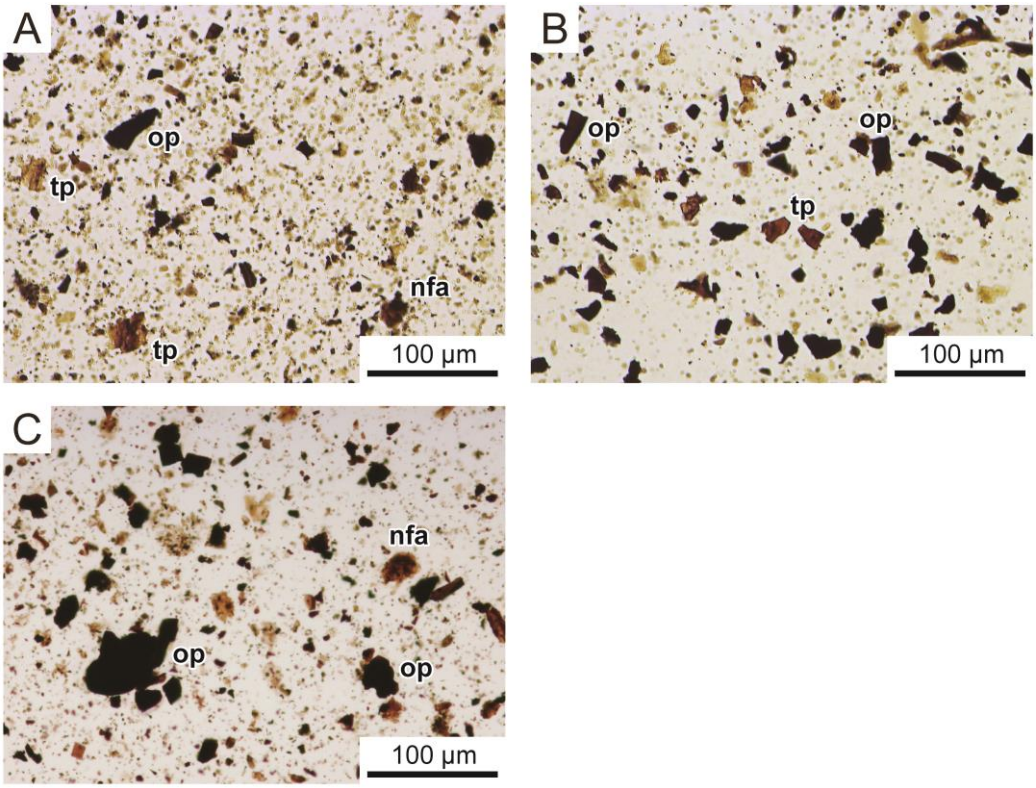

265

266 **Fig. 4.** Photomicrographs of kerogen extracted from selected samples: (A) CS21, (B) CS52, and (C)

267 CS59. tp: translucent phytoclasts; op: opaque phytoclasts; nfa: non-fluorescent amorphous organic

268 matter. Note that these three components dominate the SOM in each sample.

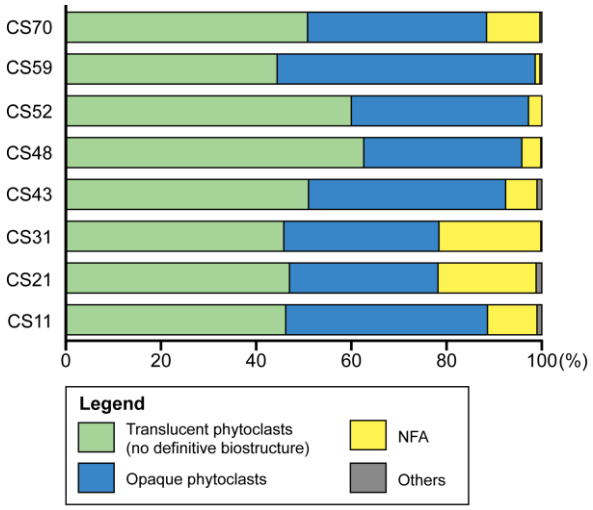

269

270 **Fig. 5**. Relative abundance (%) of various constituents of SOM extracted from eight selected samples.

271

272 **Table 2.** Relative abundance (%) of various constituents of SOM extracted from eight selected

273 samples.

Sample	Stratigraphic height (m)	Phytoclast			Amorphous organic matter			Palynomorph	
		Opaque	Translucent		NFA	WFA	FA	Pollen/Spore Grains	Phytoplankton
			No definitive biostructure	Definitive biostructure					
CS70	1195	37.6	50.8	-	11.2	-	-	0.4	-
CS59	1098	54.2	44.4	-	1.0	-	0.4	-	-
CS52	903	37.2	60.0	-	2.8	-	-	-	-
CS48	854	33.2	62.6	-	4.0	-	-	0.2	-
CS43	769	41.4	51.0	0.4	6.6	-	-	0.6	-
CS31	630	32.6	45.8	-	21.4	-	-	0.2	-
CS21	382	31.2	47.0	0.6	20.6	0.4	-	-	0.2
CS11	234	42.4	46.2	0.2	10.4	-	0.6	0.2	-

275 **Table 3.** Elemental compositions of kerogen extracted from eight selected samples.

Sample	Stratigraphic height (m)	TOC (wt%)	TH (wt%)	H/C (atomic ratio)
CS70	1195	73.26	3.74	0.61
CS59	1098	72.80	3.93	0.65
CS52	903	72.67	3.81	0.63
CS48	854	72.69	3.79	0.63
CS43	769	71.94	2.80	0.47
CS31	630	65.58	3.93	0.72
CS21	382	63.51	3.02	0.57
CS11	234	71.45	4.84	0.81

276

277 *4.2. TOC content and stable carbon isotope ratios*

278 The average TOC content was 0.52 wt% and ranged from 0.43 to 0.67 wt% (Table

279 4). Stratigraphic variations in the TOC content were relatively minor, and most values

280 were 0.5–0.6 wt% for the Senpohshi Formation (Fig. 6).

Table 4. TOC content and $\delta^{13}C_{org}$ values obtained for the Senpohshi Formation.

Sample	Stratigraphic height (m)	Age (Ma)	TOC (wt%)	$\delta^{13}C_{org}$ (‰)	Sample	Stratigraphic height (m)	Age (Ma)	TOC (wt%)	$\delta^{13}C_{org}$ (‰)
CS01	11	69.467	0.60	-25.6	CS37	679	68.544	0.57	-25.5
CS02	47	69.417	0.55	-25.7	CS38	705	68.508	0.59	-25.4
CS03	88	69.360	0.58	-25.6	CS39	716	68.493	0.61	-24.4
CS04	96	69.349	0.53	-25.6	CS40	733	68.469	0.64	-25.6
CS05	107	69.334	0.55	-25.7	CS41	748	68.448	0.55	-25.2
CS06	129	69.304	0.59	-25.8	CS42	759	68.433	0.53	-25.3
CS07	141	69.287	0.57	-25.5	CS43	769	68.419	0.56	-25.5
CS08	171	69.246	0.58	-25.9	CS44	795	68.384	0.59	-25.4
CS09	189	69.221	0.50	-25.7	CS45	809	68.364	0.59	-25.3
CS10	208	69.194	0.60	-25.9	CS46	826	68.341	0.53	-24.8
CS11	234	69.159	0.61	-25.9	CS47	837	68.326	0.55	-24.4
CS12	249	69.138	0.58	-26.1	CS48	854	68.314	0.43	-24.4
CS13	274	69.103	0.45	-25.8	CS49	872	68.307	0.52	-24.6
CS14	286	69.087	0.51	-25.9	CS50	883	68.302	0.53	-24.6
CS15	305	69.060	0.53	-25.9	CS51	893	68.297	0.50	-24.7
CS16	307	69.058	0.60	-25.7	CS52	903	68.293	0.55	-24.4
CS17	318	69.042	0.52	-25.8	CS53	910	68.290	0.62	-24.6
CS18	328	69.029	0.57	-25.8	CS54	943	68.276	0.56	-25.2
CS19	338	69.015	0.56	-25.7	CS55	958	68.269	0.50	-24.8
CS20	361	68.983	0.48	-25.7	CS56	1062	68.224	0.54	-25.2
CS21	382	68.954	0.67	-25.7	CS57	1073	68.219	0.61	-25.2
CS22	405	68.922	0.61	-25.9	CS58	1087	68.213	0.59	-25.3
CS23	438	68.877	0.57	-25.5	CS59	1098	68.208	0.58	-25.2
CS24	458	68.849	0.63	-26.3	CS60	1114	68.202	0.59	-25.3
CS25	471	68.831	0.56	-25.7	CS61	1122	68.198	0.57	-25.3
CS26	486	68.810	0.59	-25.5	CS62	1129	68.195	0.52	-25.4
CS27	499	68.792	0.50	-25.6	CS63	1143	68.189	0.60	-25.3
CS28	512	68.774	0.58	-25.5	CS64	1146	68.188	0.64	-25.7
CS29	530	68.750	0.53	-25.7	CS65	1153	68.185	0.55	-25.3
CS30	549	68.723	0.54	-25.3	CS66	1167	68.179	0.58	-25.5
CS31	630	68.611	0.47	-25.3	CS67	1177	68.174	0.58	-25.5
CS32	643	68.594	0.55	-25.4	CS68	1182	68.172	0.61	-25.1
CS33	649	68.585	0.54	-25.5	CS69	1188	68.169	0.57	-25.4
CS34	658	68.573	0.60	-25.1	CS70	1195	68.166	0.62	-25.4
CS35	665	68.563	0.57	-25.5	CS71	1251	68.142	0.56	-25.6
CS36	671	68.555	0.55	-25.5	CS72	1275	68.132	0.56	-25.4

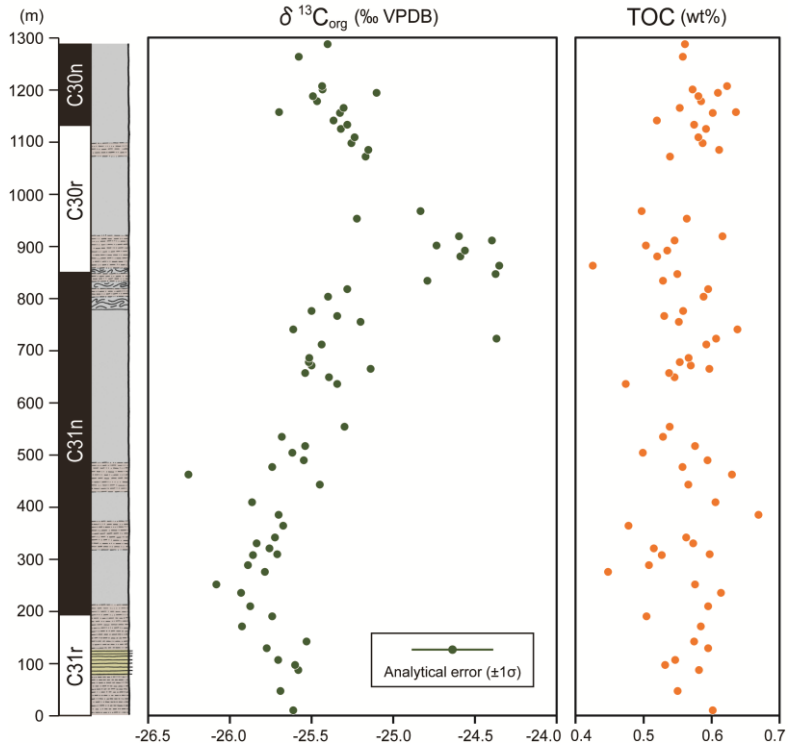

Fig. 6. Stratigraphic variation of stable carbon isotope values of bulk SOM ($\delta^{13}C_{org}$) and TOC content within the Senpohshi Formation. Error bar shows an overall uncertainty (±0.25‰: 1σ) indicated by repeated analysis of the laboratory standard.

The average stable carbon isotope value of the bulk SOM obtained from the Senpohshi Formation was –25.4‰ and ranged from –26.3 to –24.4‰ (Table 4). The stratigraphic profile compiled for the measured $\delta^{13}C_{org}$ is shown in Fig. 6. From the top of C31r to the uppermost part of C31n, $\delta^{13}C_{org}$ values are almost constant (~–25.5‰). A small negative trough appeared at the bottom of C31n (~0.5‰ in amplitude), but the amplitude of this feature was within measurement uncertainty. There is an apparent

294 negative excursion in the middle of C31n (~0.8‰ in amplitude), which is represented by
295 a single measurement point. Following this interval of approximately constant values, the
296 $\delta^{13}C_{org}$ profile showed a distinct positive excursion at the C30r/C31n boundary (from ~–
297 25.5 to ~–24.5‰). The stable carbon isotope values declined across C30r before
298 recovering to background values (~–25.5‰) at the bottom of C30n.
299
300 **5. Discussion**
301 *5.1. Origin and diagenesis of SOM*
302 The SOM within the Senpohshi Formation is dominated by phytoclasts with a minor
303 amount of NFA, which together account for more than 99% of the SOM (Fig. 5, Table 2).
304 Previous studies have proposed that phytoclasts originated from terrestrial higher plants
305 (Tyson, 1995), as did NFA (Sawada and Akiyama, 1994; Watanabe and Akiyama, 1998;
306 Omura and Hoyanagi, 2004). Sawada and Akiyama (1994) reached this conclusion based
307 on an analysis of a high NFA content sample from the Toarcian Shale, Yorkshire, England.
308 The authors reported that the $\delta^{13}C$ value of the sample was equivalent to the $\delta^{13}C$ values
309 of terrestrial higher plants, and the density of the SOM was similar to that of vitrinite.
310 Watanabe and Akiyama (1998) and Omura and Hoyanagi (2004) reached the same
311 conclusions based on analyses of carbon isotope values of high NFA content samples

312 from the Niigata sedimentary basin, central Japan. The authors showed that $\delta^{13}C$ values
313 of the SOM were equivalent to those of terrestrial higher plants, and they suggested that
314 the NFA originated from terrestrial higher plants. In the case of the Senpohshi Formation,
315 irrespective of the NFA content, stable carbon isotope values of the bulk SOM range from
316 –26.3 to –24.4‰ (Table 4), which coincides with the $\delta^{13}C$ values of terrestrial higher C3
317 plants (Deines, 1980; Jasper and Gagosian, 1990; Whelan and Thompson-Rizer, 1993).
318 These results indicate that the SOM from the Senpohshi Formation originated from
319 terrestrial higher plants.

320 The atomic H/C ratios obtained from the extracted kerogen samples from the
321 Senpohshi Formation were used to estimate the degree of thermal diagenesis. The $\delta^{13}C$
322 composition of woody material is modified from its original value via an isotopic
323 exchange reaction with carbonate during the graphitization stage of metamorphism
324 (>400 °C) (Dunn and Valley, 1992). In contrast, the $\delta^{13}C$ composition of woody material
325 is not significantly altered by hydrocarbon generation that occurs before metamorphism
326 (Deines, 1980; Teerman and Hwang, 1991; Whiticar, 1996). The atomic H/C ratios of the
327 kerogen samples from the Senpohshi Formation, which range from 0.47 to 0.81, indicate
328 that the coalification rank of the kerogen is largely below the anthracite stage, although
329 some kerogen samples could be classified to be of early anthracite stage (Table 3)

330 (Teichmüller and Teichmüller, 1979). Five of the eight extracted kerogen samples yielded
331 small numbers of pollen/spore grains, supporting our interpretation that the thermal
332 diagenesis of the kerogen resulted in the material below the anthracite stage (Table 2).
333 These observations indicate that the thermal diagenesis of the Senpohshi Formation was
334 less than that corresponding to the graphitization stage of metamorphism. Therefore, it is
335 suggested that the $\delta^{13}C$ values the SOM were not modified by thermal diagenesis.

336 To summarize, our analysis indicates that the $\delta^{13}C_{org}$ values obtained for the
337 Senpohshi Formation represent the original values of the carbon isotope composition of
338 terrestrial higher plants.

339

340 *5.2. Comparison of the carbon isotope stratigraphy with other sections*

341 The carbon isotope stratigraphy of the middle of the Maastrichtian is characterized
342 by the MME, which consists of two positive peaks separated by a negative trough with
343 short-term negative excursions (Batenburg et al., 2018; Jung et al., 2012; Voigt et al.,
344 2012). The three segments of the event are labelled MME1 to MME3 in ascending order
345 in this study, after the zonation by Voigt et al., (2012).

346 Previous research suggested two possibilities for age correlation of the MME (Fig.
347 7). Batenburg et al. (2018) correlated the event based on the cyclostratigraphy of the

348 Zumaia section in northern Spain and the IODP Site U1403 in the Newfoundland Margin.
349 They identified the event in the Maastrichtian 405 kyr cycles from the upper $Ma_{405}9$ to
350 lower $Ma_{405}5$, corresponding to 69.38 Ma through 67.87 Ma (~1,510 kyr in duration).
351 Another interpretation was proposed by Voigt et al. (2012) from the magnetostratigraphy
352 of the Gubbio section, Italy. They distinguished the event in the lower part of the polarity
353 chron C31n. It is correlated to 69.21 Ma through 68.63 Ma (~580 kyr in duration)
354 according to the astronomically calibrated Maastrichtian magnetostratigraphy by Husson
355 et al. (2011) (Option 2). Thibault et al. (2012b) suggested a similar view based on the
356 magnetostratigraphy and cyclostratigraphy of the ODP Site 762C in Indian Ocean. They
357 implied the event in the lower C31n (upper $Ma_{405}8$ through upper $Ma_{405}7$); however, it
358 was not confirmed by carbon isotope data because they interpreted the event within a
359 missing section.
360

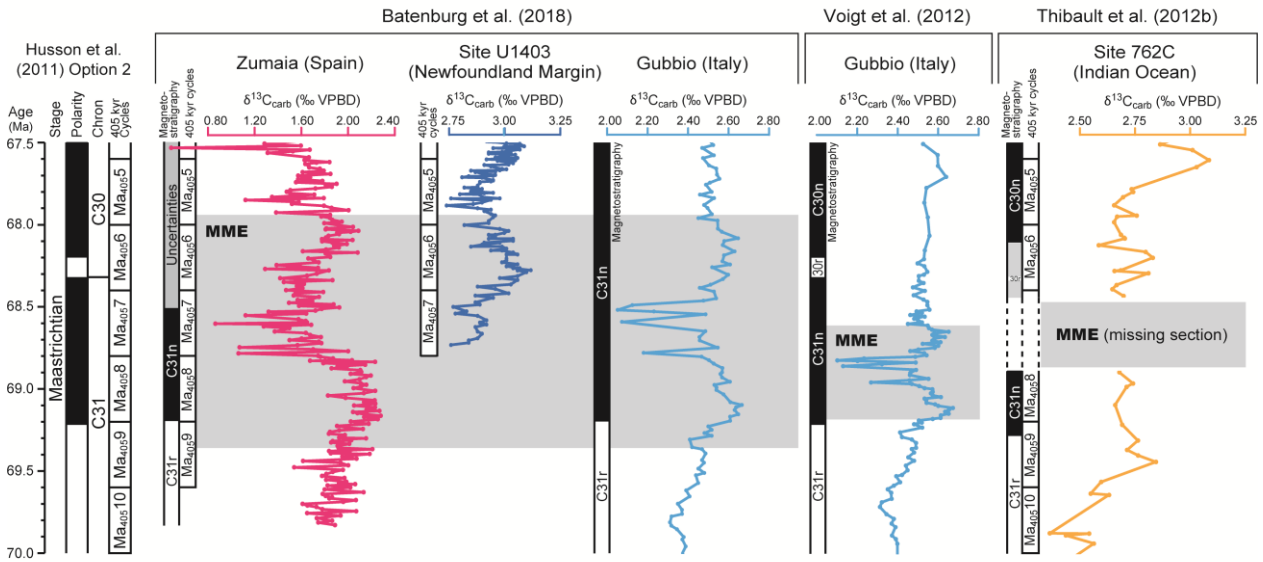

Fig. 7. Comparison of the age model for the MME after Thibault et al. (2012b), Voigt et al. (2012), and Batenburg et al. (2018). Ages were adjusted to the astronomically calibrated Maastrichtian time scale by Husson et al. (2011) (Option 2).

Comparing the two hypothesis described above, the age model by Batenburg et al. (2018) provides better agreement among the carbon isotope profiles from multiple sections. Reliable stratigraphic correlation has been established between the Zumaia section and Site U1403 based on cyclostratigraphy, and the carbon isotope profiles during the MME are consistent each other. Moreover, the positive peaks recognized in the $Ma_{405}6$ at the Site 762C can be correlated to the upper positive peak of the event in the Zumaia section and Site U1403, although Thibault et al. (2012b) originally placed the peaks above the MME. Batenburg et al. (2018) implied uncertainty in the

374 magnetostratigraphy of the Gubbio section, and they made a stratigraphic correlation by
375 using tie-points in the carbon isotope curve. The results showed a good agreement of the
376 carbon isotope profile from the Gubbio section with the other sections. The above
377 observations suggest the age correlation by the Batenburg et al. (2018) is more
378 appropriate because of better consistency of carbon isotope curves among multiple
379 sections.

380 Therefore, this study follows the age model for the MME proposed by Batenburg et
381 al. (2018). It is indicated that the carbon isotope stratigraphy of the Senpohshi Formation
382 covers the stratigraphic level right below the MME through the uppermost part of the
383 event (Figs. 6 and 7). Based on this age model, the carbon isotope profile from the
384 Senpohshi Formation was correlated to other sections (Fig. 1). Six sections representing
385 marine carbon isotope records were selected, namely the Gubbio section in Italy (Voigt
386 et al., 2012), the Zumaia section in northern Spain (Batenburg et al., 2012), Equatorial
387 Pacific ODP Site 1210B (Jung et al., 2012), Indian Ocean ODP Site 762C (Thibault et al.,
388 2012b), South Atlantic DSDP Site 525A (Li and Keller, 1998), and Newfoundland
389 Margin IODP Site U1403 (Batenburg et al., 2018). Bulk carbonate samples were analyzed
390 at these sections except for Site 525A, where they examined single species foraminifera
391 samples. The terrestrial carbon isotope records had been obtained from the Naiba section,

392 Sakhalin, Eastern Russia (Hasegawa et al., 2003), the lower Cantwell Formation, Alaska,
393 US (Salazar-Jaramillo et al., 2016), and the Aguja, Javelina, and Black Peaks Formations
394 in the Tornillo Basin, Texas, US (Nordt et al., 2003). The carbon isotope profiles were
395 derived from terrestrial organic matter in the Naiba section and Cantwell Formation.
396 Pedogenic carbonate was investigated in the Tornillo Basin. Ages of all the selected
397 sections were adjusted to the astronomically calibrated Maastrichtian time scale by
398 Husson et al. (2011) (Option 2). Stratigraphic correlations were made after
399 cyclostratigraphy (Zumaia, Site U1403, and Site 762C), magnetostratigraphy (Senpohshi
400 Formation, Site 525A, and Naiba) (Table 5), or tie-points in the carbon isotope profile
401 (Gubbio, Site 1210B, Cantwell Formation, and Tornillo Basin). The tie-points were after
402 Voigt et al. (2012) and Batenburg et al. (2018) (Table 6), and the carbon isotope curves
403 from the four sections were correlated to the Zumaia section. The results of the
404 comparison of the carbon isotope stratigraphy of the Senpohshi Formation with other
405 sections are shown in Fig. 8.
406
407 **Table 5.** Ages of the K-Pg boundary and the Maastrichtian polarity chron boundaries after Option 2
408 proposed by Husson et al. (2011).

Event	Age (Ma)
K/PgB	66 ± 0.07

C29r/C30n	66.3 ± 0.08
C30n/C30r	68.2 ± 0.08
C30r/C31n	68.32 ± 0.07
C31n/C31r	69.22 ± 0.07
C31r/C32n1n	71.4 ± 0.08

409

410 **Table 6.** Tie-points for correlation of stable carbon isotope profiles, which are defined by Voigt et al.

411 (2012) and Batenburg et al. (2018).

Tie-point	Description	Reference
V2	$\delta^{13}C$ minimum a short distance below the C29r/C30n boundary	Voigt et al. (2012)
V3a	$\delta^{13}C$ maximum within C30n, transition towards long-term d13C decline	Voigt et al. (2012)
V4	Upper $\delta^{13}C$ max of the mid-Maastrichtian $\delta^{13}C$ plateau	Voigt et al. (2012)
B3	the δ13C minimum within a broad plateau of high δ13C values in the mid-Maastrichtian, within C31n	Batenburg et al. (2018)
V5	Inflection towards the lower $\delta^{13}C$ maximum of the mid-Maastrichtian $\delta^{13}C$ plateau, a short distance above the C31n/C31r boundary	Voigt et al. (2012)
V6	Inflection towards the long-term Maastrichtian $\delta^{13}C$ rise in C31r, top of the CMBE, top occurrence of *Tranolithus orionatus*	Voigt et al. (2012)

412

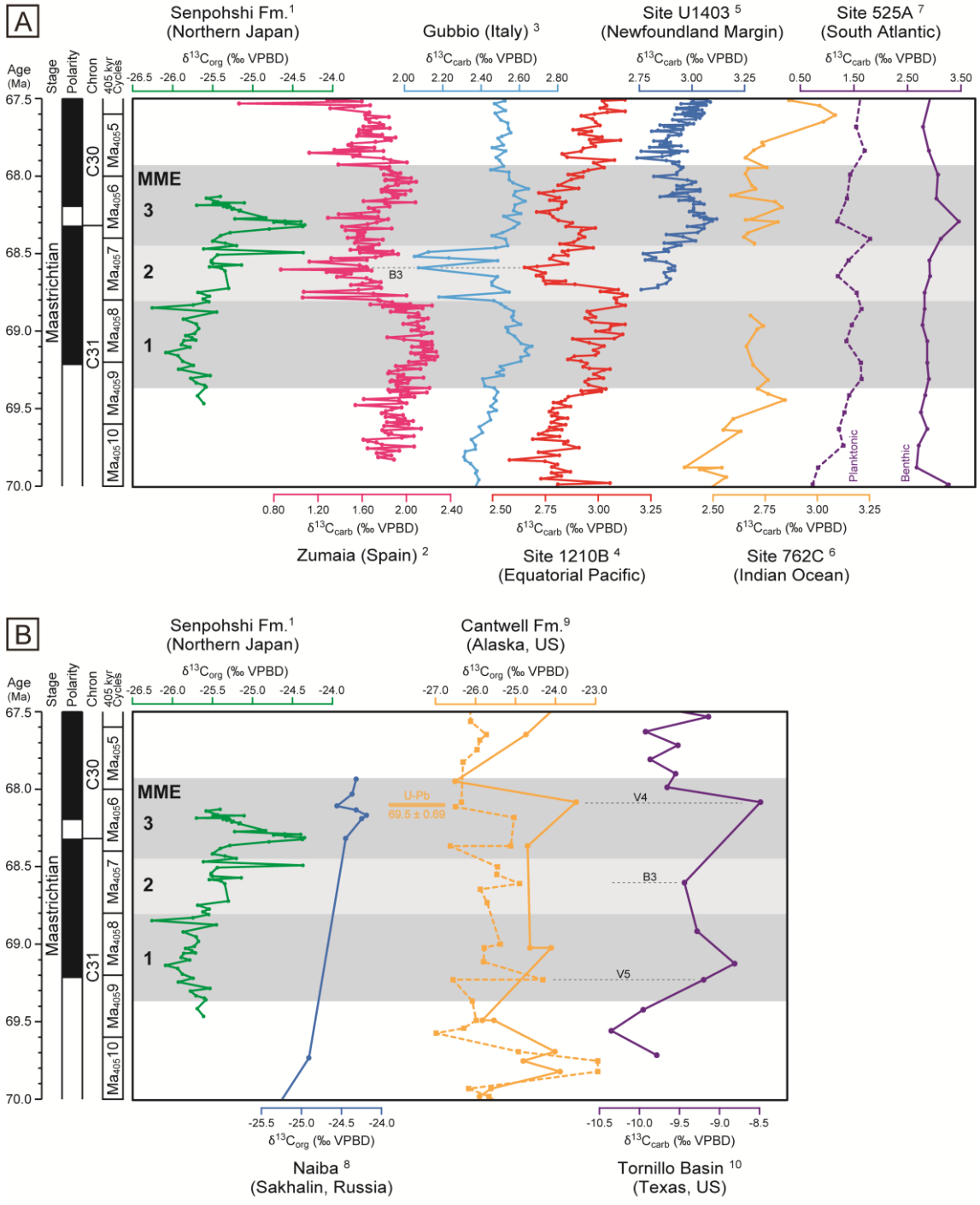

413

414 **Fig. 8.** Correlation of stable carbon isotope stratigraphy of the Senposhi Formation with other sections.

415 (A) Correlation with carbon isotope profiles obtained from marine materials. (1) Senpohshi Formation

416 of the Nemuro Group, northern Japan (this study); (2) Zumaia section, Basque country, Northern Spain

(Batenburg et al., 2012); (3) Bottaccione Gorge and the Contessa Highway sections at Gubbio, Italy (Voigt et al., 2012); (4) ODP Site 1210B, Equatorial Pacific (Jung et al., 2012); (5) IODP Site U1403, Newfoundland Margin (Batenburg et al., 2018); (6) ODP Site 762C, Indian Ocean (Thibault et al., 2012b); (7) DSDP Site 525A, South Atlantic (Li and Keller, 1998). Bulk carbonate was analyzed at these sites except for the DSDP Site 525A, where they measured single-species planktonic (Rugoglobigerina rugosa) and benthic foraminifera (Anomalinoides acufa). (B) Correlation with carbon isotope profiles obtained from terrestrial materials. (8) Naiba section, Sakhalin, eastern Russia (Hasegawa et al., 2003). Bulk sedimentary organic matter was analyzed. (9) lower Cantwell Formation, Alaska, US (Salazar-Jaramillo et al., 2016). Stable carbon isotope compositions were obtained from bulk sedimentary organic matter and fossil wood. (10) Aguja, Javelina, and Black Peaks Formations in the Tornillo Basin, Texas, US (Nordt et al., 2003). They measured pedogenic carbonate. Astronomically calibrated magnetostratigraphy and the 405 kyr eccentricity cycles are after Option 2 of Husson et al. (2011). The light and dark gray shaded intervals correspond to the MME and its constituting segments after Voigt et al. (2012).

The MME is widely recognized in the marine carbon isotope records (Fig. 8A) (e.g., Voigt et al., 2010; Thibault et al., 2012a; Voigt et al., 2012; Jung et al., 2012; Wendler et al., 2011; Wendler, 2013; Batenburg et al., 2018). Recently acquired high-resolution data

435 from Zumaia, Gubbio, Site 1210B, and Site U1403 provided detailed features of the
436 carbon isotope profile during the event (Batenburg et al., 2012; Jung et al., 2012; Voigt
437 et al., 2012; Batenburg et al., 2018). All the sections conformably show the three segments
438 of the event, which consist of two positive peaks intercalated by a negative trough with
439 short-term negative excursions.

440 In contrast, there remains uncertainty in identification of the MME and its
441 constituting segment in the terrestrial records, because of the limitation of data resolution
442 and age control. The presence of the MME was suggested by the terrestrial records from
443 the lower Cantwell Formation and Tornillo Basin (Fig. 8B) (Nordt et al., 2003; Salazar-
444 Jaramillo et al., 2016). The identification of the event largely relied on the features of the
445 carbon isotope curves. Positive peaks in the two sections showed an apparent similarity
446 to the positive peaks in the segments MME1 and MME3 recognized in the marine records.
447 However, their presence is less confident because each peak is represented by a single
448 measurement point. Moreover, the two sections lack sufficient age control to correlate the
449 carbon isotope profiles to the MME. A bentonite U-Pb zircon age of 69.5 ± 0.69 Ma was
450 indicated near the second positive peak in the lower Cantwell Formation (Salazar-
451 Jaramillo et al., 2016). However, the measured age is not fully consistent with the age of
452 the segment MME3 (68.45 Ma – 67.86 Ma) after the age model by Batenburg et al. (2018).

There is no stratigraphic marker in the Maastrichtian interval in the Tornillo Bain, even though the KPg boundary had been indicated by a weak iridium anomaly in the studied section (Lehman, 1990; Nordt et al., 2003).

Therefore, higher resolution data from the Senpohshi Formation with age control by magnetostratigraphy has significance in the recognition of the MME in the terrestrial record. The terrestrial record of the MME in the Senpohshi Formation suggests both similarity and difference to the marine carbon isotope records (Fig. 8A). Both records show a positive peak in the segment MME3. The Senpohshi Formation shows a positive excursion at the C30r/C31n boundary which is consistent with the peak at the same stratigraphic level at the Sites 1210B and U1403. The excursion can also be correlated with a small positive peak near the C30r/C31n boundary at the Sites 525A and 762C, though it is represented by a single measurement point (Li and Keller, 1998; Thibault et al., 2012b). In the segment MME2, both Senpohshi Formation and marine records show negative shift of the carbon isotope value from the overlying segment. The marine records also illustrate multiple short-term negative excursions superimposed on the negative trough; however, they are not clear in the Senpohshi Formation. A negative peak at 68.85 Ma could be correlated to one of the short-term negative excursions in other sections, though there is uncertainty in the recognition of the peak because it is represented by a

single measurement point. Lower resolution of the data in the segment MME2 of the Senpohshi Formation possibly caused the lack of short-term negative excursions in the carbon isotope profile. In contrast, there is a clear discrepancy between the Senposhi Formation and the other sections in the segment MME1. The marine records show a positive peak in this interval; however, the Senpohshi Formation indicates a slight negative shift of the carbon isotope values. The difference might suggest local factors affecting carbon isotope values recorded in the Senpohshi Formation.

In summary, this study provides the first high-resolution terrestrial carbon isotope record of the MME which is comparable to the high-resolution data from marine materials. The results indicate the carbon isotopic signatures defined by the marine records are recognized in the terrestrial materials, especially in the middle to upper part of the event (segments MME2 and MME3). However, the terrestrial data of the Formation showed a discrepancy from the marine records in the lower part of the event (segment MME1), suggesting influence of local factors in the study area. We will discuss the factors in the following section.

5.3. Factors influencing carbon isotope profile recorded in the Senpohshi Formation

The terrestrial organic matter-derived carbon isotope data of the Senpohshi Formation showed a discrepancy from the marine records in the lower part of the MME (Fig. 8A). The difference is seemingly caused by local factors of the Formation. There are some potential factors that can affect carbon isotope values of the terrestrial organic matter: (1) compositional changes in terrestrial organic matter, (2) reworking of older sediment, and (3) changes in the hinterland environment.

Regarding the Factor 1, it is unlikely that compositional changes in terrestrial organic matter preserved in sediment contributed to the carbon isotope profile of the Senpohshi Formation because the composition of terrestrial organic matter did not change significantly. The SOM in the Senpohshi Formation is dominated by opaque and translucent phytoclasts and a minor amount of NFA (Fig. 6 and Table 2). The relative abundance of the three macerals in the samples from the segment MME1 (kerogen samples CS11 and CS21) was within the range of the abundances in the overlaying segments (kerogen samples CS31, CS43, CS48, CS52, CS59, and CS70). These observations indicate that a change in terrestrial organic matter composition is unlikely to cause the deviation of the carbon isotope profile.

504 It is also difficult to explain the discrepancy through reworking of terrestrial organic
505 matter from older sediment (Factor 2). Although the interval contains thin layers of
506 sediment-gravity-flow deposits and thin slump deposits (Fig. 6), sampling sites of
507 specimens were chosen to avoid gravity flow deposits. The upper interval of the
508 Formation also contains gravity flow deposits. However, the data from the upper interval
509 shows a positive carbon isotope excursion which can be globally correlated to the positive
510 peak in other sections (Fig. 8). The data from the upper interval indicates the sampling
511 method avoided the influence of reworking materials.
512 A possible cause for the discrepancy is a changing hinterland environment (Factor
513 3). Stable carbon isotope values of terrestrial plants are affected by abiotic factors of the
514 environment of these plants, such as relative humidity, temperature, precipitation, soil
515 moisture, and atmospheric CO_2 concentration (e.g., Farquhar et al., 1980; Ramesh et al.,
516 1986; Körner et al., 1988; Leavitt, 1993; Feng and Epstein, 1995; Lipp et al., 1996;
517 Pendall et al., 1999; Schleser et al., 1999; Edwards et al., 2000). The carbon isotope
518 profiles also reflect plant species variation (Lloyd and Farquhar, 1994; Chikaraishi and
519 Naraoka, 2003), which can be caused by a changing hinterland environment. In addition,
520 a large-scale shift of the sediment source area may change plant species composition
521 delivered to the depositional sites. However, it is not likely in the study area because the

522 sediments were sourced from restricted area of the adjacent island arc (Kiminami, 1983;
523 Kimura, 1994; Fujiwara et al., 1995). Therefore, it is suggested that changes in the
524 hinterland environment and floral assemblage affected the carbon isotope values recorded
525 in the Senpohshi Formation during the early phase of the MME.

526 The discrepancy of the carbon isotope profiles among the Senpohshi Formation and
527 the other sections suggests spatial variation of paleoenvironment during the early phase
528 of the MME. Additional paleoenvironmental research should illuminate the nature and
529 cause of the local variation of the terrestrial environment in the North Pacific region. This
530 study provides new insight into environmental changes during the late Maastrichtian by
531 establishing a detailed carbon isotope record of terrestrial materials.

532

533 **6. Conclusions**

534 High-resolution stable carbon isotope stratigraphy of terrestrial organic matter was
535 established for the upper Maastrichtian Senpohshi Formation of the Nemuro Group of
536 eastern Hokkaido, northern Japan. Geochemical and petrographic analyses of bulk SOM
537 and extracted kerogen samples led to the following conclusions:

538 (1) The SOM within the Senpohshi Formation is dominated by phytoclasts and a minor
539 amount of NFA. Because both phytoclasts and NFA are interpreted to have originated

from terrestrial higher plants, the SOM within the Senpohshi Formation is inferred to have the same origin.

(2) The atomic H/C ratios obtained for the extracted kerogen samples range from 0.47 to 0.81, indicating a coalification rank at the anthracite stage or below. This finding reveals that $\delta^{13}C_{org}$ values obtained from the Senpohshi Formation were not significantly varied by thermal diagenesis. Therefore, the $\delta^{13}C_{org}$ values obtained for the Senpohshi Formation represent the original values of the carbon isotope composition of terrestrial higher plants.

(3) The stable carbon isotope profile reconstructed for the Formation provides the first high-resolution terrestrial record of the MME, which is comparable to high-resolution marine carbon isotope data. The carbon isotopic signatures defined by the marine records are recognized in the terrestrial data from the Formation, especially in middle to upper part of the event. However, the terrestrial record showed a discrepancy from the marine data in the lower part of the MME, suggesting local variation of the hinterland environment in the North Pacific region. This study provides new insight into environmental changes during the late Maastrichtian by establishing a detailed carbon isotope record of terrestrial materials.

7. Acknowledgments

We are grateful to Toshifumi Komatsu and Takeshi Matsunaga for their help with sampling in the field, Takashi Hasegawa for providing instructions regarding carbon isotope analysis, and Atsushi Ando for guidance on palynological techniques and helpful discussions. We acknowledge the use of facilities kindly made available by Naoto Ishikawa, Kazufumi Yazaki, and the Research Institute for Humanity and Nature. We are indebted to the staff at the Akkeshi Marine Station of Hokkaido University, who supported us during fieldwork. This study was performed under the cooperative research program of the Center for Advanced Marine Core Research (CMCR) of Kochi University (accept numbers 05B021 and 06B017). The study was supported in part by a Sasakawa Scientific Research Grant awarded by The Japan Science Society (grant number 20-752M). This research was also partially funded by Sediment Dynamics Research Consortium. We are grateful for the financial support from: INPEX, JAPEX, JOGMEC, and JX. We sincerely thank two anonymous reviewers for their insightful and constructive comments.

8. References

Arthur, M.A., Fischer, A.G., 1977. Upper Cretaceous-Paleocene magnetic stratigraphy at Gubbio, Italy. I. Lithostratigraphy and sedimentology. Geological Society of America Bulletin 88, 367–371.

Asano, K., 1962. Japanese Paleogene from the view-point of foraminifera with descriptions of several new species. Contributions Institute of Geology and Paleontology, Tohoku University 57, 1–32. (in Japanese, with English Abstract)

Barrera, E., Huber, B.T., 1990. Evolution of Antarctic waters during the Maastrichtian: Foraminifer oxygen and carbon isotope ratios, Leg 113. Proceedings of the Ocean Drilling Program, Scientific Results 113, 813–827.

Barrera, E., Savin, S.M., 1999. Evolution of late Campanian-Maastrichtian marine climates and oceans. In: Barrera, E., Johnson, C.C. (Eds.), Evolution of the Cretaceous ocean-climate system. Geological Society of America Special Paper 332, p. 245–282.

Barrera, E., Savin, S.M., Thomas, E., Jones, C.E., 1997. Evidence for thermohaline-circulation reversals controlled by sea-level change in the latest Cretaceous. Geology 25, 715–718.

591 Batenburg, S. J., Sprovieri, M., Gale, A. S., Hilgen, F. J., Hüsing, S., Laskar, J., Liebrand,
592 D., Lirer, F., Orue-Etxebarria, X., Pelosi, N., Smit, J., 2012. Cyclostratigraphy and
593 astronomical tuning of the Late Maastrichtian at Zumaia (Basque country, Northern
594 Spain). Earth and Planetary Science Letters, 359, 264-278.
595 Batenburg, S. J., Friedrich, O., Moriya, K., Voigt, S., Cournède, C., Moebius, I., Blum, P.,
596 Bornemann, A., Fiebig, J. Hasegawa, T., Hull, P. M., Norris, R. D., Röhl, U., Sexton,
597 P. F., Westerhold, T. Wilson, P. A., the IODP Expedition 342 Scientists, 2018. Late
598 Maastrichtian carbon isotope stratigraphy and cyclostratigraphy of the
599 Newfoundland Margin (Site U1403, IODP Expedition 342). Newsletters on
600 Stratigraphy, 51, 245-260.
601 Bazhenov, M.L., Burtman, V.S., 1994. Upper Cretaceous paleomagnetic data from
602 Shikotan Island, Kuril Arc: Implications for plate kinematics. Earth and Planetary
603 Science Letters 122, 19–28.
604 Bazhenov, M.L., Zharov, A.E., Levashova, N.M., Kodama, K., Bragin, N.Y., Fedorov, P.I.,
605 Bragina, L.G. Lyapunov, S.M., 2001. Paleomagnetism of a Late Cretaceous island
606 arc complex from South Sakhalin, East Asia: Convergent boundaries far away from
607 the Asian continental margin? Journal of Geophysical Research: Solid Earth, 106,
608 19193-19205.

609 Bowman, V. C., Francis, J. E., Riding, J. B., 2013. Late Cretaceous winter sea ice in
610 Antarctica?. Geology, 41, 1227-1230.
611 Burnett, J.A., 1998. Upper Cretaceous, In: Bown, P.R. (Ed.), Calcareous nannofossil
612 biostratigraphy. Campman and Hall, London, p. 132–199.
613 Caron, M., 1985. Cretaceous planktic foraminifera. In: Bolli, H.M., Saunders, J.B., Perch-
614 Nielsen, K. (Eds.), Plankton stratigraphy. Cambridge University Press, Cambridge,
615 p. 17–86.
616 Chave, A.D., 1984. Lower Paleocene-Upper Cretaceous magnetostratigraphy, Sites 525,
617 527, 528, and 529, Deep Sea Drilling Project Leg 74. Initial Reports of the Deep
618 Sea Drilling Project DSDP 74, 525-531.
619 Chikaraishi, Y., Naraoka, H., 2003. Compound-specific δD–δ^{13}C analyses of n-alkanes
620 extracted from terrestrial and aquatic plants. Phytochemistry, 63, 361-371.
621 Corfield, R.M., Norris, R.D., 1996. Deep water circulation in the Paleocene ocean.
622 Geological Society, London, Special Publications, 101, 443–456.
623 Corfield, R.M., Cartlidge, J.E., Premoli-Silva, I., Housley, R.A., 1991. Oxygen and
624 carbon isotope stratigraphy of the Palaeogene and Cretaceous limestones in the
625 Bottaccione Gorge and the Contessa Highway sections, Umbria, Italy. Terra Nova,
626 3, 414–422.

627 Crampton, J.S., Schiøler, P., Roncaglia, L., 2006. Detection of Late Cretaceous eustatic
628 signatures using quantitative biostratigraphy. Geological Society of America
629 Bulletin, 118, 975-990.
630 Dameron, S.N., Leckie, R.M., Clark, K., MacLeod, K.G., Thomas, D.J., Lees, J.A., 2017.
631 Extinction, dissolution, and possible ocean acidification prior to the
632 Cretaceous/Paleogene (K/Pg) boundary in the tropical Pacific. Palaeogeography,
633 Palaeoclimatology, Palaeoecology, 485, 433-454.
634 Deines, P., 1980. The isotopic composition of reduced organic carbon. In: Frits, P., Fontes,
635 J.C. (Eds.), Handbook of Environmental Isotope Geochemistry 1. Elsevier,
636 Amsterdam, p. 329–406.
637 D'Hondt, S., Lindinger, M., 1994. A stable isotopic record of the Maastrichtian ocean-
638 climate system: South Atlantic DSDP site 528. Palaeogeography, Palaeoclimatology,
639 Palaeoecology, 112, 363–378.
640 Dickens, G.R., O'Neil, J.R., Rea, D.K. Owen, R.M., 1995. Dissociation of oceanic
641 methane hydrate as a cause of the carbon isotope excursion at the end of the
642 Paleocene. Paleoceanography and Paleoclimatology, 10, 965-971.

643 Donnadieu, Y., Pierrehumbert, R., Jacob, R., Fluteau, F., 2006. Modelling the primary
644 control of paleogeography on Cretaceous climate. Earth and Planetary Science
645 Letters, 248, 426-437.
646 Dunn, S.R., Valley, J.W., 1992. Calcite-graphite isotope thermometry: a test for
647 polymetamorphism in marble, Tudor gabbro aureole, Ontario, Canada. Journal of
648 Metamorphic Geology 10, 487–501.
649 Edwards, T.W.D., Graf, W., Trimborn, P., Stichler, W., Lipp, J., Payer, H.D., 2000. $\delta^{13}C$
650 response surface resolves humidity and temperature signals in trees. Geochimica et
651 Cosmochimica Acta 64, 161–167.
652 Falzoni, F., Petrizzo, M.R., Clarke, L.J., MacLeod, K.G., Jenkyns, H. C., 2016. Long-
653 term Late Cretaceous oxygen-and carbon-isotope trends and planktonic
654 foraminiferal turnover: A new record from the southern midlatitudes. Bulletin, 128,
655 1725-1735.
656 Farnsworth, A., Lunt, D.J., O'Brien, C.L., Foster, G.L., Inglis, G.N., Markwick, P.,
657 Pancost, R.D., Robinson, S.A., 2019. Climate sensitivity on geological timescales
658 controlled by nonlinear feedbacks and ocean circulation. Geophysical Research
659 Letters, 46, 9880-9889.

660 Farquhar, G. D., 1980. Carbon isotope discrimination by plants: Effects on carbon dioxide
661 concentration and temperature via the ratio of intercellular and atmospheric CO_2
662 concentrations, In: Pearman G.I. (Ed.), Carbon dioxide and climate: Australian
663 research. Australian Academy of Science, Canberra, p. 105–110.
664 Feng, X., Epstein, S., 1995. Carbon isotopes of trees from arid environments and
665 implications for reconstructing atmospheric CO_2 concentration. Geochimica et
666 Cosmochimica Acta, 59, 2599-2608.
667 Frank, T.D., Arthur, M.A., 1999. Tectonic forcings of Maastrichtian ocean-climate
668 evolution. Paleoceanography 14, 103–117.
669 Frank, T.D., Thomas, D.J., Leckie, R.M., Arthur, M.A., Bown, P.R., Jones, K., Lees, J.A.,
670 2005. The Maastrichtian record from Shatsky Rise (northwest Pacific): A tropical
671 perspective on global ecological and oceanographic changes. Paleoceanography 20,
672 PA1008.
673 Friedrich, O., Herrle, J.O., Wilson, P.A., Cooper, M.J., Erbacher, J., Hemleben, C., 2009.
674 Early Maastrichtian carbon cycle perturbation and cooling event: Implications from
675 the South Atlantic Ocean. Paleoceanography, 24, PA2211.
676 Fujiwara, Y., Kanamatsu, T., Nanayama, F., 1995. Tectonic evolution of two paleo arc-
677 trench systems in Hokkaido, northern Japan. Geofísica Internacional, 34, 283-291.

678 Gardin, S., Galbrun, B., Thibault, N., Coccioni, R., Premoli-Silva, I., 2012. Bio-
679 magnetochronology for the upper Campanian–Maastrichtian from the Gubbio area,
680 Italy: New results from the Contessa Highway and Bottaccione sections.
681 Newsletters on Stratigraphy 45, 75–104.
682 Haq, B.U., Hardenbol, J., Vail, P.R., 1987. Chronology of fluctuating sea levels since the
683 Triassic. Science 235, 1156–1167.
684 Hasegawa, T., Pratt, L.M., Maeda, H., Shigeta, Y., Okamoto, T., Kase, T., Uemura, K.,
685 2003. Upper Cretaceous stable carbon-isotope stratigraphy of terrestrial organic
686 matter from Sakhalin, Russian Far East: a proxy for the isotopic composition of
687 paleoatmospheric CO_2. Palaeogeography, Palaeoclimatology, Palaeoecology 215,
688 179–182.
689 Hay, W.W., DeConto, R., Wold, C.N., Wilson, K.M., Voigt, S., Schulz, M., Wold-Rossby,
690 A., Dullo, W.-C., Ronov, A.B., Balukhovsky, A.N., Soeding E., 1999, Alternative
691 global Cretaceous paleogeography, In: Barrera, E. and Johnson, C. (Eds.), The
692 evolution of Cretaceous ocean/climate systems, Geological Society of America
693 Special Paper 332, p. 1–47.

694 Haynes, S. J., MacLeod, K. G., Ladant, J. B., Guchte, A. V., Rostami, M. A., Poulsen, C.
695 J., Martin, E. E., 2020. Constraining sources and relative flow rates of bottom waters
696 in the Late Cretaceous Pacific Ocean. Geology, 48, 509-513.
697 Hesselbo, S.P., Robinson, S.A., Surlyk, F. Piasecki, S., 2002. Terrestrial and marine
698 extinction at the Triassic-Jurassic boundary synchronized with major carbon-cycle
699 perturbation: A link to initiation of massive volcanism?. Geology, 30, 51–254.
700 Huber, B.T., 1992. Paleobiogeography of Campanian-Maastrichtian foraminifera in the
701 southern high latitudes. Palaeogeography, Palaeoclimatology, Palaeoecology 92,
702 325–360.
703 Huber B.T., Watkins, D.K., 1992. Biogeography of Campanian-Maastrichtian calcareous
704 plankton in the region of the Southern Ocean: paleogeographic and paleoclimatic
705 implications, In: Kennett, J.P., Warnke, D.A. (Eds.), The Antarctic
706 paleoenvironment: A perspective on global change. Antarctic Research Series 56.
707 American Geophysical Union, Washington, D.C., p. 31–60.
708 Huber, B.T., Norris, R.D., MacLeod, K.G., 2002. Deep-sea paleotemperature record of
709 extreme warmth during the Cretaceous. Geology 30, 123–126.
710 Hsü, K.J., He, Q., McKenzie, J.A., Weissert, H., Perch-Nielsen, K., Oberhänsli, H., Kelts,
711 K., LaBrecque, J., Tauxe, L., Krähenbühl, U., Percival, S.F., Wright, R., Karpoff,

712 A.M., Petersen, N., Tucker, P., Poore, R.Z., Gombos, A.M., Pisciotto, K., Carman,
713 M.F., Schreiber, E., 1982. Mass mortality and its environmental and evolutionary
714 consequences. Science, 216, 249-256.
715 Hunter, S. J., Valdes, P. J., Haywood, A. M., Markwick, P. J., 2008. Modelling
716 Maastrichtian climate: investigating the role of geography, atmospheric CO 2 and
717 vegetation. Climate of the past discussions, 4, 981-1019.
718 Husson, D., Galbrun, B., Laskar, J., Hinnov, L.A., Thibault, N., Gardin, S., Locklair, R.E.,
719 2011. Astronomical calibration of the Maastrichtian (Late Cretaceous). Earth and
720 Planetary Science Letters 305, 328–340.
721 Immenhauser, A., Holmden, C., Patterson, W.P., 2008. Interpreting the carbon isotope
722 record of ancient epeiric seas: lessons from the Recent. In: Pratt, B.R., Holmden, C.
723 (Eds.), Dynamic of Epiric Seas. Geological Association of Canada, Special Paper,
724 p. 135–174
725 Isaza-Londoño, C., MacLeod, K.G., Huber, B.T., 2006. Maastrichtian North Atlantic
726 warming, increasing stratification and foraminiferal paleobiology at three
727 timescales. Paleoceanography 21, PA1012.

728 Jasper, J.P., Gagosian, R.B., 1990. The sources and deposition of organic matter in the
729 Late Quaternary Pigmy Basin, Gulf of Mexico. Geochimica et Cosmochimica Acta
730 54, 1117–1132.
731 Jenkyns, H.C., 1998. The Early Toarcian (Jurassic) Anoxic Event: stratigraphic,
732 sedimentary, and geochemical evidence, American Journal of Science 288, 101–
733 151.
734 Johnson, C.C., Kuffman, E.G., 1990. Originations, radiations and extinctions of
735 Cretaceous rudistid bivalve species in the Caribbean Province, In: Kauffman E.G.,
736 Walliser, O.H. (Eds.), Extinction events in Earth history. Springer-Verlag, New York,
737 p. 305–324.
738 Johnson, C.C., Kuffman, E.G., 1996. Maastrichtian extinction patterns of Caribbean
739 province rudistids, In: MacLeod N., Keller. G. (Eds.), Cretaceous-Tertiary boundary
740 mass extinction: Biotic and environmental changes. Norton, New York, p. 231–274.
741 Johnson, C.C., Barron, E.J., Kauffman, E.G., Arthur, M.A., Fawcett, P.J., Yasuda, M.K.,
742 1996. Middle Cretaceous reef collapse linked to ocean heat transport. Geology 24,
743 376–380.

744 Jung, C., Voigt, S., Friedrich, O., 2012. High-resolution carbon-isotope stratigraphy
745 across the Campanian–Maastrichtian boundary at Shatsky Rise (tropical Pacific).
746 Cretaceous Research 37, 177–185.
747 Jung, C., Voigt, S., Friedrich, O., Koch, M.C., Frank, M., 2013. Campanian-Maastrichtian
748 ocean circulation in the tropical Pacific, Paleoceanography, 28, 562–573.
749 Katagiri, T., Naruse, H., Ishikawa, N., Hirata, T., 2020. Collisional bending of the western
750 Paleo‐Kuril Arc deduced from paleomagnetic analysis and U–Pb age
751 determination. Island Arc, 29, e12329.
752 Keller, G., Lindinger, M., 1989. Stable isotope, TOC and CaCO3 record across the
753 Cretaceous/Tertiary boundary at El Kef, Tunisia. Palaeogeography,
754 Palaeoclimatology, Palaeoecology, 73, 243-265.
755 Kiminami, K., 1978. Stratigraphic re-examination of the Nemuro Group. Chikyu Kagaku
756 32, 120–132. (in Japanese with English abstract)
757 Kiminami, K., 1983. Sedimentary history of the late Cretaceous-Paleocene Nemuro
758 Group, Hokkaido, Japan: a forearc basin of the Paleo-Kuril arc-trench system.
759 Journal of the Geological Society of Japan 89, 607–624.

760 Kimura, G., 1994. The latest Cretaceous–Early Paleogene rapid growth of accretionary
761 complex and exhumation of high pressure series metamorphic rocks in northwestern
762 Pacific margin. Journal of Geophysical Research: Solid Earth, 99, 22147-22164.
763 Kominz, M.A., Browning, J.V., Miller, K.G., Sugarman, P.J., Mizintseva, S., Scotese,
764 C.R., 2008. Late Cretaceous to Miocene sea-level estimates from the New Jersey
765 and Delaware coastal plain coreholes: an error analysis. Basin Research 20, 211–
766 226.
767 Körner, C., Farquhar, G.D., Roksandic, Z., 1988. A global survey of carbon isotope
768 discrimination in plants from high altitude. Oecologia, 74, 623–632.
769 Ladant, J.B., Poulsen, C.J., Fluteau, F., Tabor, C.R., MacLeod, K.G., Martin, E.E., Haynes,
770 S.J., Rostami, M.A., 2020. Paleogeographic controls on the evolution of Late
771 Cretaceous ocean circulation. Climate of the Past, 16, 973-1006.
772 Leavitt, S.W., 1993. Environmental information from $^{13}C/^{12}C$ ratios of wood, In: Swart,
773 P.K., Lohmann, K.C., Mckenzie, J., Savin, S. (Eds.), Climate Change in Continental
774 Isotopic Records, Geophysical Monograph 78, 325–331.
775 Lehman, T., 1990, Paleosols and the Cretaceous/Tertiary transition in the Big Bend region
776 of Texas: Geology, 18, 362–364.

Lees, J.A., 2002. Calcareous nannofossil biogeography illustrates palaeoclimate change in the Late Cretaceous Indian Ocean. Cretaceous Research 23, 537–634.

Li, L., Keller, G., 1998. Maastrichtian climate, productivity and faunal turnovers in planktic foraminifera in South Atlantic DSDP sites 525A and 21. Marine Micropaleontology 33, 55–86.

Li, L., Keller, G., 1999 Variability in Late Cretaceous and deep waters: evidence from stable isotopes. Marine Geology 161, 171–190.

Lipp, J., Trimborn, P., Edwards, T., Waisel, Y. Yakir, D., 1996. Climatic effects on the $\delta^{18}O$ and $\delta^{13}C$ of cellulose in the desert tree Tamarix jordanis. Geochimica et Cosmochimica Acta, 60, 3305–3309.

Lloyd, J., Farquhar, G.D., 1994. 13C discrimination during CO_2 assimilation by the terrestrial biosphere. Oecologia 99, 201–215.

Lowrie, W., Alvarez, W., 1977. Upper Cretaceous-Paleocene Magnetic Stratigraphy at Gubbio, Italy. 3. Upper Cretaceous Magnetic Stratigraphy. Geological Society of America Bulletin 88, 374–377.

Lowrie, W., Alvarez, W., 1981. 100 Million Years of geomagnetic polarity history. Geology 9, 392–397.

794 MacLeod, K.G., Huber, B.T., 1996. Reorganization of deep ocean circulation
795 accompanying a Late Cretaceous extinction event. Nature 380, 422–425.
796 MacLeod, K.G., Huber, B.T., 2001. The Maastrichtian record at Blake Nose (western
797 North Atlantic) and implications for global palaeoceanographic and biotic changes,
798 In: Kroon, D., Norris, R.D., Klaus, A. (Eds.), Western North Atlantic Palaeogene
799 and Cretaceous Palaeoceanography. Goglogical Society of London Special
800 Publications 193, p. 111–130.
801 MacLeod, K.G., Huber, B.T., Ward, P.D., 1996. The biostratigraphy and
802 paleobiogeography of Maastrichtian inoceramids, In: Ryder, G., Fastovsky, D.,
803 Garter, S. (Eds.), The Cretaceous-Tertiary event and other catastrophes in Earth
804 history. Geological Society of America Special Paper 307, p. 361–373.
805 MacLeod, K.G., Huber, B.T., Ducharme, M.L., 2000. Paleontological and geochemical
806 constraints on the deep ocean during the Cretaceous greenhouse interval, In: Huber,
807 B.T., MacLeod, K.G., Wing, S.L., (Eds.), Warm climates in Earth history.
808 Cambridge University Press, Cambridge, p. 241–274.
809 MacLeod, K.G., Huber, B.T., Isaza-Londoño, C., 2005. North Atlantic warming during
810 global cooling at the end of the Cretaceous. Geology 33, 437–440.

MacLeod, K.G., Londoño, C.I., Martin, E.E., Berrocoso, Á.J., Basak, C., 2011. Changes in North Atlantic circulation at the end of the Cretaceous greenhouse interval. Nature Geoscience, 4, 779-782.

Maeda, H., Shigeta, Y., 2005. Maastrichtian ammonoid fauna from the Pugachevo area, southern Sakhalin, Russian Far East, In: Shigeta, Y., Maeda, H. (Eds.), The Cretaceous System in the Makarov area, Southern Sakhalin, Russian Far East. National Science Museum Monographs 31, National Science Museum, Tokyo, Japan, p. 121–136.

Maeda, H., Shigeta, Y., Fernando, A.G.S., Okada, H., 2005. Stratigraphy and fossil assemblages of the Upper Cretaceous System in the Makarov area, Southern Sakhalin, Russian Far East, In: Shigeta, Y., Maeda, H. (Eds.), The Cretaceous System in the Makarov area, Southern Sakhalin, Russian Far East. National Science Museum Monographs 31, National Science Museum, Tokyo, Japan, p. 25–120.

Moiroud, M., Pucéat, E., Donnadieu, Y., Bayon, G., Guiraud, M., Voigt, S., Deconinck, J.F., Monna, F., 2016. Evolution of neodymium isotopic signature of seawater during the Late Cretaceous: Implications for intermediate and deep circulation. Gondwana Research, 36, 503-522.

828 Murphy, D.P., Thomas, D.J., 2012. Cretaceous deep-water formation in the Indian sector
829 of the Southern Ocean, Paleoceanography, 27, PA1211.
830 Naruse, H., 2003. Cretaceous to Paleocene depositional history of North-Pacific
831 subduction zone: reconstruction from the Nemuro Group, eastern Hokkaido,
832 northern Japan. Cretaceous Research 24, 55–71.
833 Naruse, H., Maeda, H., Shigeta, Y., 2000. Newly discovered Late Cretaceous molluscan
834 fossils and inferred K/T boundary in the Nemuro Group, eastern Hokkaido, northern
835 Japan. Journal of the Geological Society of Japan 106, 161–164. (in Japanese with
836 English abstract)
837 Nifuku, K., Kodama, K., Shigeta, Y., Naruse, H., 2009. Faunal turnover at the end of the
838 Cretaceous in the North Pacific region: Implications from combined
839 magnetostratigraphy and biostratigraphy of the Maastrichtian Senpohshi Formation
840 in the eastern Hokkaido Island, northern Japan. Palaeogeography,
841 Palaeoclimatology, Palaeoecology 271, 84–95.
842 Nordt, L., Atchley, S., Dworkin, S., 2003. Terrestrial evidence for two greenhouse events
843 in the latest Cretaceous. GSA Today 13, 4–9.
844 Okada, H., Yamada, M., Matsuoka, H., Murota, T., Isobe, T., 1987. Calcareous
845 nannofossils and biostratigraphy of the Upper Cretaceous and Lower Paleogene

Nemuro Group, eastern Hokkaido, Japan. Journal of the Geological Society of Japan 93, 329–348.

Omura, A., Hoyanagi, K., 2004. Relationships between composition of organic matter, depositional environments, and sea-level changes in backarc basins, central Japan. Journal of Sedimentary Research 74, 620–630.

Perch-Nielsen, K., McKenzie, J., He, Q., 1982. Biostratigraphy and isotope stratigraphy and the 'catastrophic' extinction of calcareous nannoplankton at the Cretaceous/Tertiary boundary. In: Silver, L.T., Schultz, P.H. (Eds.), Geological implications of impacts of large asteroids and comets on the Earth, GSA Special Paper, 190, 353-371

Pendall, E., Betancourt, J.L., Leavitt, S.W., 1999. Paleoclimatic significance of δD and $\delta^{13}C$ values in pinon pine needles from packrat middens spanning the last 40,000 years. Palaeogeography, Palaeoclimatology, Palaeoecology, 147, 53-72.

Pospichal, J.J., Wise Jr, S.W., 1990. Maestrichtian calcareous nannofossil biostratigraphy of Maud Rise, ODP Leg 113 Sites 689 and 690, Weddell Sea. Proceedings of Ocean Drilling Project, Scientific Results 113, 465–487.

862 Pucéat, E., Donnadieu, Y., Ramstein, G., Fluteau, F., Guillocheau, F., 2005. Numerical
863 evidence for thermohaline circulation reversals during the Maastrichtian, Geochem.
864 Geophys. Geosyst., 6, Q11012.
865 Ramesh, R., Bhattacharya, S.K. and Gopalan, K., 1986. Climatic correlations in the stable
866 isotope records of silver fir (*Abies pindrow*) trees from Kashmir, India. Earth and
867 Planetary Science Letters, 79, 66-74.
868 Robinson, S.A., Vance, D., 2012. Widespread and synchronous change in deep-ocean
869 circulation in the North and South Atlantic during the Late Cretaceous,
870 Paleoceanography, 27, PA1102.
871 Robinson, S.A., Murphy, D.P., Vance, D., Thomas, D.J., 2010. Formation of "southern
872 component water" in the Late Cretaceous: evidence from Nd-isotopes. Geology, 38,
873 871-874.
874 Salazar-Jaramillo, S., Fowell, S.J., McCarthy, P.J., Benowitz, J.A., Śliwiński, M.G.
875 Tomsich, C.S., 2016. Terrestrial isotopic evidence for a Middle-Maastrichtian
876 warming event from the lower Cantwell Formation, Alaska. Palaeogeography,
877 Palaeoclimatology, Palaeoecology, 441, 360-376.

878 Sawada, K., Akiyama, M., 1994. Carbon isotope composition of macerals separated from
879 various kerogens by density separation method. Journal of the Japanese Association
880 for Petroleum Technology 59, 244–255. (in Japanese with English abstract)
881 Schleser, G.H., Helle, G., Lücke, A. Vos, H., 1999. Isotope signals as climate proxies: the
882 role of transfer functions in the study of terrestrial archives. Quaternary Science
883 Reviews, 18, 927–943.
884 Shafik, S., 1990. Late Cretaceous nannofossil biostratigraphy and biogeography of the
885 Australian western margin. Bureau of Mineral Resources, Geology and Geophysics
886 Report 295, 1–164.
887 Shigeta, Y., Nishimura, T., Nifuku, K., 2015. Middle and late Maastrichtian (latest
888 Cretaceous) ammonoids from the Akkeshi Bay area, eastern Hokkaido, northern
889 Japan and their biostratigraphic implications. Paleontological Research 19, 107–127.
890 Scholle, P.A. & Arthur, M.A. 1980. Carbon-isotope fluctuations in Cretaceous pelagic
891 limestones: potential stratigraphic and petroleum exploration tool. AAPG Bulletin,
892 64, 67–87
893 Simmons, M.D., Sharland, P.R., Casey, D.M., Davies, R.B., Sutcliffe, O.E., 2007. Arabian
894 Plate sequence stratigraphy: Potential implications for global chronostratigraphy.
895 GeoArabia, 12, 101-130.

896 Stoll, H.M., Schrag, D.P., 2000. High-resolution stable isotope records from the upper
897 cretaceous rocks of Italy and Spain: glacial episodes in a greenhouse planet?
898 Geological Society of America. Bulletin 112, 308–319.
899 Teerman, S.C., Hwang, R.J., 1991. Evaluation of the liquid hydrocarbon potential of coal
900 by artificial maturation techniques. Organic Geochemistry, 17, 749-764.
901 Teichmuller, M., Teichmuller, R., 1979. Diagenesis of coal (coalification), In: Larsen, G.,
902 Chilingar, G.V. (Eds.), Diagenesis in Sediments and Sedimentary Rocks. Elsevier,
903 Amsterdam, p. 207–246.
904 Thibault, N., Gardin, S., 2006. Maastrichtian calcareous nannofossil biostratigraphy and
905 paleoecology in the Equatorial Atlantic (Demerara Rise, ODP Leg 207 Hole 1258A).
906 Revue de Micropaléontologie, 49, 199-214.
907 Thibault, N., Gardin, S., 2007. The late Maastrichtian nannofossil record of climate
908 change in the South Atlantic DSDP Hole 525A. Marine Micropaleontology 65, 163–
909 184.
910 Thibault, N., Gardin, S., 2010. The calcareous nannofossil response to the end-Cretaceous
911 warm event in the Tropical Pacific. Palaeogeography, Palaeoclimatology,
912 Palaeoecology 291, 239–252.

913 Thibault, N., Gardin, S., Galbrun, B., 2010. Latitudinal migration of calcareous
914 nannofossil *Micula murus* in the Maastrichtian: implecationsfor globas climate
915 change. Geology 38, 203–206.
916 Thibault, N., Harlou, R., Schovsbo, N., Schiøler, P., Minoletti, F., Galbrun, B., Lauridsen,
917 B.W., Sheldon, E., Stemmerik, L., Surlyk, F., 2012a. Upper Campanian–
918 Maastrichtian nannofossil biostratigraphy and high-resolution carbon-isotope
919 stratigraphy of the Danish Basin: towards a standard δ13C curve for the Boreal
920 Realm. Cretaceous Research 33, 72–90.
921 Thibault, N., Husson, D., Harlou, R., Gardin, S., Galbrun, B., Huret, E., Minoletti, F.,
922 2012b. Astronomical calibration of upper Campanian–Maastrichtian carbon isotope
923 events and calcareous plankton biostratigraphy in the Indian Ocean (ODP Hole
924 762C): implication for the age of the Campanian–Maastrichtian boundary.
925 Palaeogeography, Palaeoclimatology, Palaeoecology 337, 52–71.
926 Thibault, N., Harlou, R., Schovsbo, N.H., Stemmerik, L. Surlyk, F., 2016. Late
927 Cretaceous (late Campanian–Maastrichtian) sea-surface temperature record of the
928 Boreal Chalk Sea. Climate of the Past, 12, 429-438.
929 Tobin, T.S., Ward, P.D., Steig, E.J., Olivero, E.B., Hilburn, I.A., Mitchell, R.N., Diamond,
930 M.R., Raub, T.D., Kirschvink, J.L., 2012. Extinction patterns, $\delta^{18}O$ trends, and

magnetostratigraphy from a southern high-latitude Cretaceous–Paleogene section: Links with Deccan volcanism. Palaeogeography, Palaeoclimatology, Palaeoecology, 350–352, 180–188.

Toshimitsu, S., Matsumoto, T., Noda, M., Nishida, T., Maiya, S., 1995. Towards an integrated mega-, micro- and magneto-stratigraphy of the Upper Cretaceous in Japan. Journal of the Geological Society of Japan 101, 19–29. (in Japanese with English abstract)

Tyson, R.V., 1995. Sedimentary Organic Matter: Organic Facies and Palynofacies. Champman and Hall, Lodnon. 633 p.

Uramoto, G. I., Tahara, R., Sekiya, T., Hirano, H., 2013. Carbon isotope stratigraphy of terrestrial organic matter for the Turonian (Upper Cretaceous) in northern Japan: Implications for ocean-atmosphere δ13C trends during the mid-Cretaceous climatic optimum. Geosphere, 9, 355–366.

Voigt, S., Friedrich, O., Norris, R.D., Schoenfeld, J., 2010. Campanian–Maastrichtian carbon isotope stratigraphy: shelf-ocean correlation between the European shelf sea and the tropical Pacific Ocean. Newsletters on Stratigraphy 44, 57–72.

Voigt, S., Gale, A.S., Jung, C., Jenkyns, H.C., 2012. Global correlation of Upper Campanian–Maastrichtian successions using carbon-isotope stratigraphy:

949 development of a new Maastrichtian timescale. Newsletters on Stratigraphy 45, 25–
950 53.
951 Ward, P.D., Kennedy, W.J., MacLeod, K.G., Mount, J.F., 1991. Ammonite and inoceramid
952 bivalve extinction patterns in Cretaceous/Tertiary boundary sections of the Biscay
953 region (southwestern France, northern Spain). Geology 19, 1181–1184.
954 Watanabe, H., Akiyama, M., 1998. Characterization of organic matter in the Miocene
955 turbidites and hemipelagic mudstones in the Niigata oil field, central Japan. Organic
956 Geochemistry 29, 605–611.
957 Wendler, I., 2013. A critical evaluation of carbon isotope stratigraphy and biostratigraphic
958 implications for Late Cretaceous global correlation. Earth-Science Reviews, 126,
959 116–146.
960 Wendler, I., Willems, H., Gräfe, K.-U., Ding, L., Luo, H., 2011. Upper Cretaceous
961 interhemispheric correlation between the Southern Tethys and the Boreal: chemo-
962 and biostratigraphy and paleoclimatic reconstructions from a new section in the
963 Tethys Himalaya, S-Tibet. Newsletters on Stratigraphy 44, 137–171.
964 Whelan J.K., Thompson-Rizer, C.L., 1993. Chemical methods for assessing kerogen and
965 protokerogen types and maturity, In: Engel, M.H., Macko, S. (Eds.), Organic
966 Geochemistry, Principles and Applications. Plenum Press, New York, p. 289–353.

Whiticar, M.J., 1996. Stable isotope geochemistry of coals, humic kerogens and related natural gases. International Journal of Coal Geology, 32, 191-215.

Yamada, M., 1984. Calcareous nannoflssils and planktonic foraminifera from the west coast of the Akkeshi Bay, Hokkaido, In: Saito, T., Okada H., Kaiho, K. (Eds.), Biostratigraphy and international correlation of the Paleogene System in Japan. Faculty of Science, Yamagata University, Yamagata, Japan, p. 15–18. (in Japanese)

Zachos, J.C., Arthur, M.A., 1986. Paleoceanography of the Cretaceous/Tertiary boundary event: inferences from stable isotopic and other data. Paleoceanography 1, 5–26.

Zachos, J. C., Arthur, M. A., Thunell, R. C., Williams, D. F., Tappa, E. J.,1985. Stable isotope and trace element geochemistry of carbonate sediments across the Cretaceous/Tertiary boundary at Deep Sea Drilling Project Hole 577, Leg 861. Initial Reports of the Deep Sea Drilling Project 86, 513–532.

Zachos, J. C., Arthur, M. A., Dean, W. E., 1989. Geochemical evidence for suppression of pelagic marine productivity at the Cretaceous/Tertiary boundary. Nature, 337, 61–64.

9. Figure captions

985 **Fig. 1.** Paleogeographic map of the late Maastrichtian (68 Ma; modified after Hay et al.,
986 1999, https://www.odsn.de/odsn/services/paleomap/adv_map.html) showing the location
987 of the sections used in this study. SN: Senphoshi Formation of the Nemuro Group,
988 northern Japan; NB: Naiba section, Sakhalin, eastern Russia; GB: Bottaccione Gorge and
989 the Contessa Highway sections at Gubbio, Italy; Zumaia section, Basque country,
990 Northern Spain; TR: Aguja, Javelina, and Black Peaks Formations in the Tornillo Basin,
991 Texas, US; CT: lower Cantwell Formation, Alaska, US. Numbers indicate DSDP, ODP,
992 and IODP sites (DSDP Site 525A, South Atlantic Ocean; ODP Site 762C, Indian Ocean;
993 ODP Site 1210B, equatorial Pacific Ocean; IODP Site U1403, Newfoundland Margin).
994
995 **Fig. 2.** Index maps showing (A) the location of Hokkaido, (B) the distribution of the
996 Nemuro Group, and (C) location of the studied section.
997
998 **Fig. 3.** Lithology and magnetostratigraphy (after Nifuku et al., 2009) of the Senpohshi
999 Formation. Correlation with the astronomically calibrated magnetostratigraphic time
1000 scale (Option 2 of Husson et al., 2011) is shown. Stratigraphic position of the sampling
1001 sites is also indicated in the figure.
1002

Fig. 4. Photomicrographs of kerogen extracted from selected samples: (A) CS21, (B) CS52, and (C) CS59. tp: translucent phytoclasts; op: opaque phytoclasts; nfa: non-fluorescent amorphous organic matter. Note that these three components dominate the SOM in each sample.

Fig. 5. Relative abundance (%) of various constituents of SOM extracted from eight selected samples.

Fig. 6. Stratigraphic variation of stable carbon isotope values of bulk SOM ($\delta^{13}C_{org}$) and TOC content within the Senpohshi Formation. Error bar shows an overall uncertainty (±0.25‰: 1σ) indicated by repeated analysis of the laboratory standard.

Fig. 7. Comparison of the age model for the MME after Thibault et al. (2012b), Voigt et al. (2012), and Batenburg et al. (2018). Ages were adjusted to the astronomically calibrated Maastrichtian time scale by Husson et al. (2011) (Option 2).

Fig. 8. Correlation of stable carbon isotope stratigraphy of the Senposhi Formation with other sections. (A) Correlation with carbon isotope profiles obtained from marine

materials. (1) Senpohshi Formation of the Nemuro Group, northern Japan (this study); (2) Zumaia section, Basque country, Northern Spain (Batenburg et al., 2012); (3) Bottaccione Gorge and the Contessa Highway sections at Gubbio, Italy (Voigt et al., 2012); (4) ODP Site 1210B, Equatorial Pacific (Jung et al., 2012); (5) IODP Site U1403, Newfoundland Margin (Batenburg et al., 2018); (6) ODP Site 762C, Indian Ocean (Thibault et al., 2012b); (7) DSDP Site 525A, South Atlantic (Li and Keller, 1998). Bulk carbonate was analyzed at these sites except for the DSDP Site 525A, where they measured single-species planktonic (*Rugoglobigerina rugosa*) and benthic foraminifera (*Anomalinoides acufa*). (B) Correlation with carbon isotope profiles obtained from terrestrial materials. (8) Naiba section, Sakhalin, eastern Russia (Hasegawa et al., 2003). Bulk sedimentary organic matter was analyzed. (9) lower Cantwell Formation, Alaska, US (Salazar-Jaramillo et al., 2016). Stable carbon isotope compositions were obtained from bulk sedimentary organic matter and fossil wood. (10) Aguja, Javelina, and Black Peaks Formations in the Tornillo Basin, Texas, US (Nordt et al., 2003). They measured pedogenic carbonate. Astronomically calibrated magnetostratigraphic time scale and the 405 kyr eccentricity cycles are after Option 2 of Husson et al. (2011). The light and dark gray shaded intervals correspond to the MME and its constituting segments after Voigt et al. (2012).

10. Table captions

Table 1. Stratigraphic positions of polarity chron boundaries in the Senpohshi Formation (Nifuku et al., 2009).

Table 2. Relative abundance (%) of various constituents of SOM extracted from eight selected samples.

Table 3. Elemental compositions of kerogen extracted from eight selected samples.

Table 4. TOC content and $\delta^{13}C_{org}$ values obtained for the Senpohshi Formation.

Table 5. Ages of the K-Pg boundary and the Maastrichtian polarity chron boundaries after Option 2 proposed by Husson et al. (2011).

Table 6. Tie-points for correlation of stable carbon isotope profiles, which are defined by Voigt et al. (2012) and Batenburg et al. (2018).